JOHANNES KEPLER
UNIVERSITÄT LINZ

Submitted by

Alexander Planer

Submitted at

Linz Institute for Organic Solar Cells (LIOS)/ Institute of Physical Chemistry

Thesis Supervisor

a. Univ. Prof. Dr. Markus Scharber

Thesis Co-Supervisor

DI Katarina Gugujonović

November 2022

INVESTIGATION OF PHASE SEGREGATION IN WIDE BAND GAP PEROVSKITE SOLAR CELLS

Bachelor Thesis

to obtain the academic degree of

Bachelor of Science (BSc)

in the Bachelor program

Chemistry and Chemical Technology

JOHANNES KEPLER UNIVERSITÄT LINZ
Altenberger Straße 69
4040 Linz, Österreich
jku.at
DVR 0093696

JOHANNES KEPLER
UNIVERSITÄT LINZ

SWORN DECLARATION

I hereby declare that the thesis submitted is my own unaided work, that I have not used other than the sources indicated, and that all direct and indirect sources are acknowledged as references.

Place, date Signature

Acknowledgement

First and foremost, I would like to thank o. Univ.-Prof. Mag. Dr. DDr. h.c. Niyazi Serdar Sariciftci for not only letting me write my thesis at his institute, but more for creating the spark of interest for photovoltaic science and the motivation to pursue and conduct scientific discovery in the first place.

I would like to express my biggest thanks to my co-supervisor DI Katarina Gugujonović, for not only guiding me through my thesis, but for all the academic and moral support. Thank you for all the lengthy discussions, for all the input and considerations and for always being able to rely on you no matter what the issue was.

I would also like to thank a. Univ. Prof. Dr. Markus Scharber not only for the guidance through this thesis, but more importantly for all the help with every device used and with all the background theory. Thank you for bringing the spark of an idea into this thesis, whenever I was feeling like standing in front of a wall.

Lastly, I would like to say thank you for all my university colleagues and LIOS members that have made my time at the institute and at the JKU so wonderful. The last three years would by far not have been such a good time, if it were not for you Konstantin Siegel, BSc., Julia Bičvić, BSc., Dominik Böhm, BSc., Lisa Berger, BSc., DI Elisabeth Leeb, Nadine Kleinbruckner, BSc., DI Felix Mayr and Dr. Dominik Wielend.

Abstract

Organic inorganic halide perovskite materials have gained great interest for their use as absorber material in electrical devices such as perovskite solar cells. Due to their tuneable bandgap and their fabrication from precursor solution they possess a broad range of advantages compared to common inorganic photovoltaic devices. In this thesis the focus was the investigation of passivating wide band gap perovskite films. Hoke, et al. reported that wide band gap OIHP films show an effect called light-induced “phase segregation”, which reduces the efficiency and thus the performance of photovoltaic devices. One way to overcome this phase segregation is by using additives, of which potassium iodide, phenethyl ammonium iodide and lead thiocyanate are investigated in this study. This was done by using PL-spectroscopy and incorporating the additives into perovskite solar cells and analysing their current-voltage behaviour.

Kurzfassung

Organisch-anorganische Halogenid Perowskite rückten mehr und mehr in den Fokus von Forschern als Absorbermaterial in elektrischen Bauteilen wie Perowskit-Solarzellen. Aufgrund ihrer leicht veränderbaren Bandlücke und ihrer simplen Produktionswege aus der Lösung, besitzen sie eine Reihe an Vorteilen gegenüber herkömmlichen anorganischen Solarzellen. Der Fokus dieser Arbeit lag in der Untersuchung der Möglichkeit Perowskitfilme mit großer Bandlücke zu passivieren. Hoke, et al. fand, dass OAHP-Filme mit großer Bandlücke einen Effekt namens „Phasensegregation“ zeigen, der die Bandlücke des Materials verringert und dadurch die Effizienz von Perowskit-Bauteilen in Solarzellen verringert. Dieser Effekt kann unterdrückt werden durch Verwendung von Additiven. Von diesen Additiven werden Kaliumiodid, Phenethyl Ammoniumiodid und Blei(II)thiocyanat in dieser Arbeit untersucht.

Table of Contents

List of Abbreviations

1-BuOH	1-Butanol
1-PrOH	1-Propanol
AFM	Atomic Force Microscopy
BCP	Bathocuproine
CB	Chlorobenzene
DMF	Dimethylformamide
DMSO	Dimethyl Sulfoxide
ETL	Electron Transport Layer
EtOH	Ethanol
EQE	External Quantum Efficiency
FF	Fill Factor
HCl	Hydrochloric Acid
HTL	Hole Transport Layer
IPA	Iso-Propyl Alcohol
ITO	Indium Tin Oxide
IV-Curve	Current Voltage Curve
J_{SC}	Short Circuit Current Density
LP	Long Pass
MeOH	Methanol
MeO-2PACz	[2-(3,6-Dimethoxy-9H-carbazol-9-yl)ethyl]phosphonic Acid
OIHP	Organic Inorganic Halide Perovskite
$PC_{60}BM$	[6,6]-phenyl-C61-butyric Acid Methyl Ester
PCE	Power Conversion Efficiency
PEAI	Phenethyl Ammonium Iodide
PL	Photoluminescence
PSC	Perovskite Solar Cell
PTFE	Polytetrafluoroethylene
SEM	Scanning Electron Microscopy
V_{OC}	Open Circuit Voltage
WBG	Wide Band Gap
XRD	X-Ray Diffraction

1. Introduction

With rising global energy demand and increasing awareness in CO_2-release that comes with traditional means of energy production, solar energy has gained a tremendous increase in interest as an alternative to coal, oil and gas. With a technical feasibility of delivering 3 MW of solar power for each person on this planet [1] from solar energy, this sector of energy production has gained more and more attention by both governments and scientists. With the ongoing improvement of solar cell technology, and record breaking 47.1% [2] efficiency in multi-junction solar cells, photovoltaic technology has become a potential game changer in the global energy market.

One of the emerging solar cell technologies are perovskite solar cells (PSC). PSCs contain materials with a perovskite crystal structure in their centre and have some advantages over traditional silicon solar cells. For instance, they can be manufactured from their precursor solutions and have the possibility to have their band gap adjusted by varying the precursor solution composition [3].

Especially when incorporating PSCs into tandem solar cells, the threshold of about 30% power conversion efficiency (PCE) for single-junction cells can be overcome. Currently, with an efficiency of 25.8% [4], PSCs are yet an emerging technology, however, the potential ongoing research in this field shows tremendous potential for the photovoltaic industry as visible in Fig. 1.

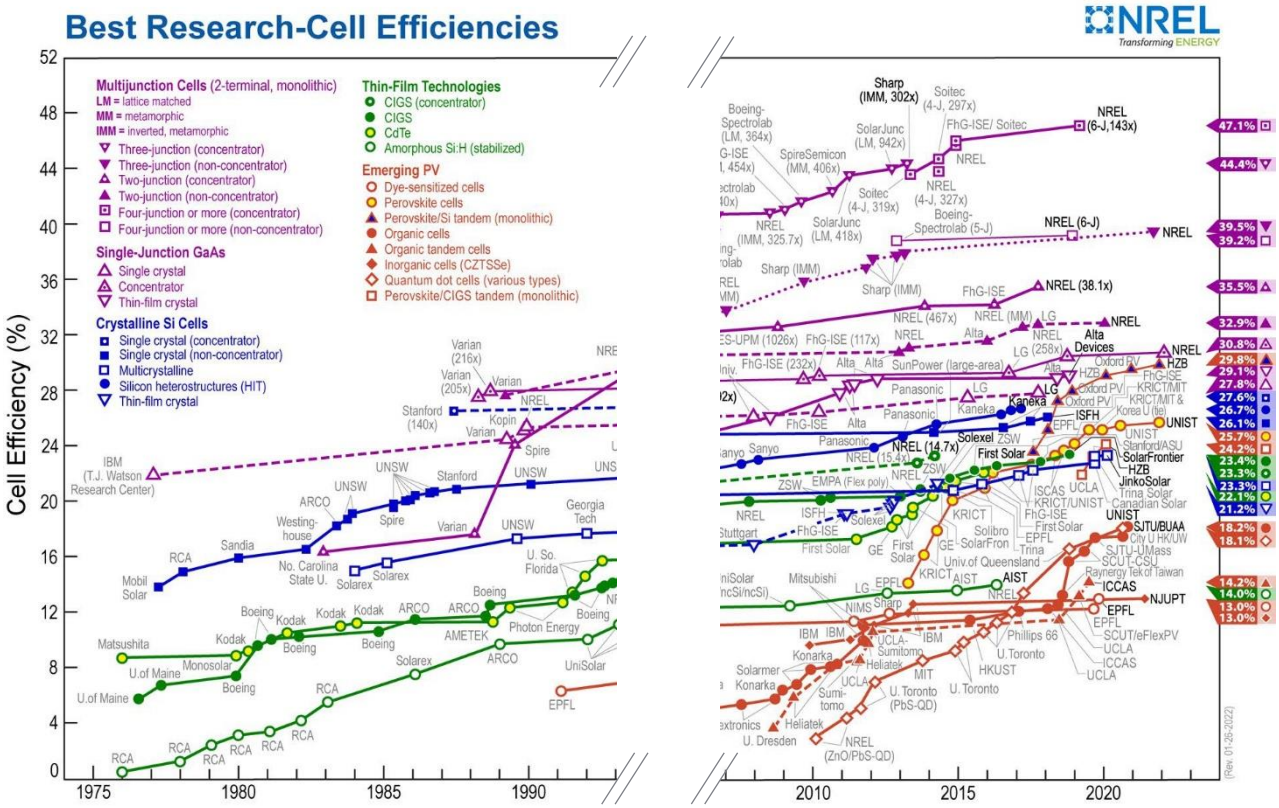

Figure 1: Current benchmark photovoltaic devices and their cell efficiencies for solar cells of various subgroups. Figure from Ref. [5].

1.1. Organic inorganic halide perovskites

Of particular interest for this study were so called organic inorganic halide perovskites (OIHP). A perovskite is a calcium titanium oxide mineral ($CaTiO_3$), which was named by Gustav Rose after the Russian mineralogist Lev Perovski (Лев Перовский) [6]. However, many materials have a perovskite crystal structure, which is described by an octahedral crystal of type ABX_3, depicted in Fig. 2. In the case of an OIHP, ***A*** stands for a small organic or inorganic cation, ***B*** describes the metal cation in the centre of the octahedron, while ***X*** describes the anions occupying the octahedral spaces around the central cation [7, 18]. In the case of this study, the central metal cation is Pb^{2+} while Br^- or I^- are used as anions. Perovskite materials of this composition not only show the property that they can absorb incoming photons and create an electron-hole pair

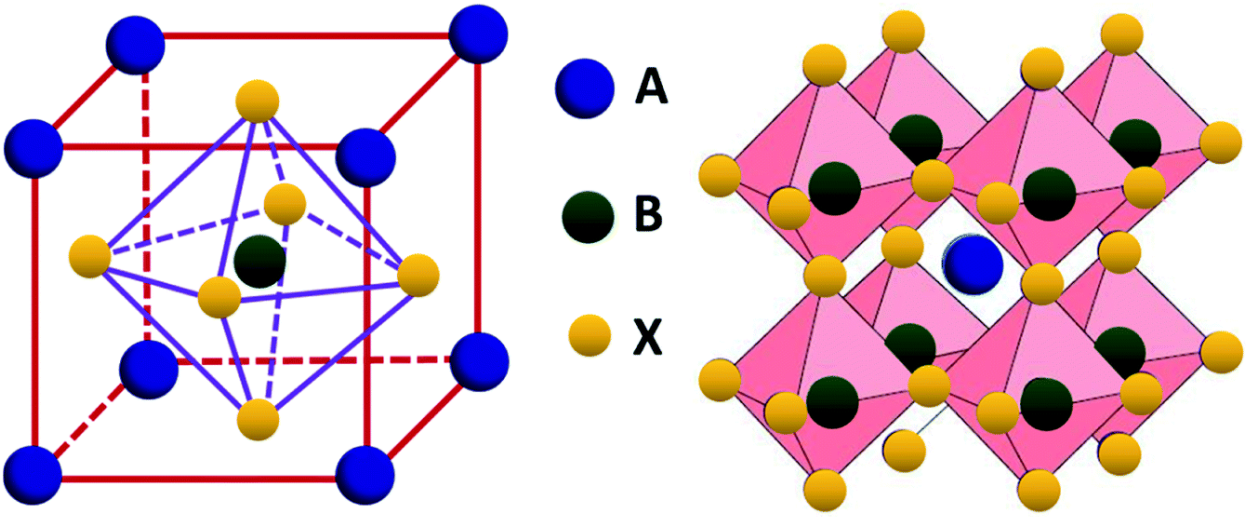

Figure 2: Structure of perovskite crystal with A being the small organic cation, B standing for the central metal cation and X for the anions. Figure from Ref. [8].

(exciton) but are remarkable for their high radiative recombination rate [9,10]. In the case that this electron-hole pair does not recombine to produce a photon but instead is collected via charge transport layers as electrical current, OIHP materials become particularly interesting for solar cells. This charge transport is supported by adding an electron transport layer (ETL) as well as a hole transport layer (HTL) to the perovskite [11,12].

Another important property of OIHP devices is the ability to tune the bandgap towards higher energies, which is useful for their incorporation into tandem solar cells. Such tandem solar cells are a technology that has a lot of potential in photovoltaic research, as it allows to surpass the threshold set by the Shockley-Queisser limit for single-junction solar cells. This limit for single-junction solar cells, which is just about 30 % PCE, has been a huge obstacle to overcome in solar cell research [15]. However, tandem solar cells are composed of two or more sub cells with complementary absorption spectra, so that the Shockley-Queisser limit for single junction cells can be surpassed [7,10,14,17].

For this to happen the two sub cells need to be designed in a way that their bandgaps complement each other in terms of light absorption from the solar spectrum, as can be seen in Fig. 3. As the overall photocurrent is limited by the lowest sub cell current, the current densities of both sub cells must match. [18,19]. For absorption in the region of shorter wavelengths a wide band gap (WBG) PSC can be used. By varying the bromide/iodide concentration, band gaps in the range of 1.5 to 2.3 eV [13,14] can be achieved.

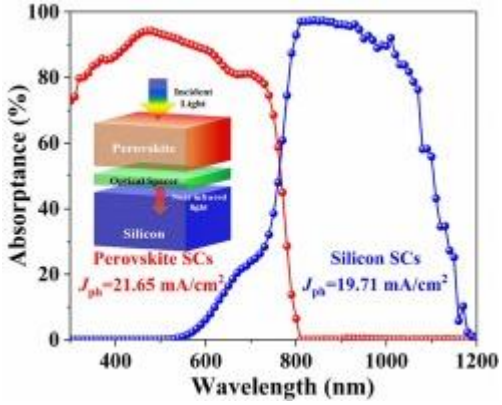

Figure 3: Complementary absorption of light for tandem solar cell with Perovskite and Silicon sub cells. Figure from Ref. [20].

1.2. Phase segregation in WBG perovskites

By partially replacing I^- anions with Br^- ions, an effect called phase segregation occurs. It was reported that upon illumination of WBG perovskite materials a second signal appears in the photoluminescence spectrum. This is thought to occur due to ionic motion of the anions to form an iodide and a bromide rich phase. As the I^--rich domain shows a smaller band gap, charge carriers will more frequently recombine via the iodide dominated region. The recombination via a smaller band gap results in a lower energetic emission. This effect has, since its first observation, also been referred to as Hoke effect, and can be detected using x-ray diffraction (XRD) or photoluminescence spectroscopy (PL-spectroscopy) [16]. However, this phase segregation is believed to be fully reversible upon leaving the perovskite material in the dark for relaxation for a few minutes [10,17]. The segregation into an I^--rich domain and a Br^--rich domain is responsible for introducing deep level traps in the crystal, which account for losses in charge carriers in perovskite materials [10,17]. Thus, the occurring phase segregation has a significant impact on performance of PSCs. It reduces for example the solar cells short circuit current density (J_{SC}), its open circuit voltage (V_{OC}), its fill factor (FF) and consequently its power conversion efficiency (PCE) [10].

One way to reduce and suppress this phase segregation is by passivation of the perovskite with certain additives [10,17]. In this thesis the main focus was laid onto potassium iodide (KI) [18,22,25], lead thiocyanate ($Pb(SCN)_2$) [23,24] as well as phenethyl ammonium iodide (PEAI) [26,27] as potential passivating agents. Because of the ionic nature of OIHP materials, three main approaches exist for the passivation of trap states and for improving both the stability and the performance of OIHP devices [10]. The first of these approaches is passivation by coordinate bonding. Especially losses caused by Pb^{2+} and I^- ions at the grain boundaries that are not fully coordinated can be decreased. A prominent agent for this approach is [6,6]-phenyl-C_{61}-butyric acid methyl ester ($PC_{60}BM$), which was used in this study as an ETL. The second approach is passivation by ionic bonding. This is mainly done to fill vacant ion sites within the perovskite crystal

by introducing ions into the system that, by their size and charge, fit into the perovskite crystal pattern. This is the case for KI as well as $Pb(SCN)_2$. The third way to suppress phase segregation is to transform the grain boundaries in perovskite crystals into a 2D-layer [10,17,28]. Lattice matching between the 2D and 3D-perovskite phases potentially passivates both the perovskite surface and the grain boundaries [10]. The possibility to form a 2D-perovskite layer is attributed to molecules like PEAI.

The aim of this thesis was to investigate the influence of passivation with the help of KI, $Pb(SCN)_2$ and PEAI on perovskite films and solar cells of composition $FA_{0.8}Cs_{0.2}Pb(I_xBr_{1-x})_3$. Further, it was investigated, how well passivation can be achieved by increasing the bromide concentration of the perovskite and thus shifting the band gap towards higher levels.

2. Experimental

2.1. List of Chemicals

Table 1: List of chemicals used within this thesis.

Material	Supplier	Purity / %	Abbreviation
1-Butanol	Sigma Aldrich	99.8	1-BuOH
1-Propanol	Sigma Aldrich	99.7	1-PrOH
Acetone	VWR Chemicals	>99.0	-
Bathocuproine	Sensient Imaging Tech.	n. I.	BCP
Chlorobenzene	Sigma Aldrich	99.8	CB
Caesium Iodide	Alfa-Aesar	99.999	CsI
Dimethylformamide	Sigma Aldrich	99.8	DMF
Dimethyl sulfoxide	Sigma Aldrich	>99.9	DMSO
Ethanol	Acros Organics	99.5	EtOH
Formamidinium Iodide	Synthesized [30]	-	FAI
Isopropyl Alcohol	VWR Chemicals	100.0	IPA
Potassium Iodide	Sigma Aldrich	-	KI
Methanol	VWR Chemicals	100	MeOH
[2-(3,6-Dimethoxy-9H-carbazol-9-yl)ethyl]phosphonic Acid	TCI	>98.0	MeO-2PACz
Lead Bromide	Sigma Aldrich	99.999	$PbBr_2$
Lead Iodide	Alfa-Aesar	99.999	PbI_2
Lead Thyocyanate	Sigma Aldrich	99.5	$Pb(SCN)_2$
[6,6]-phenyl-C61-butyric acid methyl ester	Nanostructured Carbon	-	$PC_{60}BM$
Phenethyl Ammonium Iodide	Sigma Aldrich	98.0	PEAI
Toluene	VWR Chemicals	100.0	-

2.2. Precursor Solutions

For processing of both the perovskite films as well as the solar cells, precursor solutions containing 1.08 mol L^{-1} of $FA_{0.8}Cs_{0.2}Pb(I_xBr_{1-x})_3$ were used. As solvent for all solutions a mixture of 85 Vol% Dimethylformamide (DMF) and 15 Vol% Dimethyl sulfoxide (DMSO) was used. The bromide content varied between 0% and 40% leading to solutions of composition $FA_{0.8}Cs_{0.2}PbI_3$, $FA_{0.8}Cs_{0.2}Pb(I_{0.8}Br_{0.2})_3$ as well as $FA_{0.8}Cs_{0.2}Pb(I_{0.6}Br_{0.4})_3$ respectively. All chemicals used in this study can be found in **Section 2.1**. The compositions for the precursor solutions used for 1 mL of solution can be found in tables 2-4.

Table 2: Composition of precursor solution for 1 mL of $FA_{0.8}Cs_{0.2}PbI_3$, perovskite.

Compound	Weight / mg	Volume / mL
FAI	148.58	-
PbI_2	497.89	-
CsI	56.12	-
DMF	-	850
DMSO	-	150

Table 3: Composition of precursor solution for 1 mL $FA_{0.8}Cs_{0.2}Pb(I_{0.8}Br_{0.2})_3$ perovskite.

Compound	Weight / mg	Volume / mL
FAI	148.58	-
PbI_2	348.52	-
$PbBr_2$	118.91	
CsI	56.12	-
DMF	-	850
DMSO	-	150

Table 4: Composition of precursor solution for 1 mL of $FA_{0.8}Cs_{0.2}Pb(I_{0.6}Br_{0.4})_3$ perovskite.

Compound	Weight / mg	Volume / mL
FAI	148.58	-
PbI_2	199.16	-
$PbBr_2$	237.82	
CsI	56.12	-
DMF	-	850
DMSO	-	150

For use of the additives KI was added directly to the respective precursor solutions with a concentration of 0.02 mol L^{-1}. Similarly, PEAI was added with 0.03 mol L^{-1} and $Pb(SCN)_2$ with a concentration of 0.05 mol L^{-1}. Additionally, precursor solutions with a $Pb(SCN)_2$ concentration of 0.03, 0.06 and 0.09 mol L^{-1} were prepared, the exact weight for the additives used for 1 mL of each perovskite solution is given in table 5 respectively.

Table 5: Addition of additive for 1 mL of perovskite precursor solution.

Compound	Concentration / mol L^{-1}	Weight / mg
KI	0.02	3.58
PEAI	0.03	8.07
$Pb(SCN)_2$	0.03	10.00
$Pb(SCN)_2$	0.05	15.00
$Pb(SCN)_2$	0.06	20.00
$Pb(SCN)_2$	0.09	30.00

2.3. Perovskite Films

For processing thin perovskite films 15 mm × 15 mm glass substrates coated with indium tin oxide (ITO) were used. The substrates were cleaned using toluene, a 2.1 Vol% aqueous Hellmanex©-solution, H_2O and acetone before being submerged in 2-propanol (IPA) and treated in an ultrasonic bath for approximately 15 min. Those substrates were then treated in a plasma oven with O_2 for 10 min at 100 W for etching. As a next step a 0.3 mg mL^{-1} solution of [2-(3,6-Dimethoxy-9*H*-carbazol-9-yl) ethyl]phosphonic acid (MeO-2PACz) was spin coated on top of the substrates in a glovebox atmosphere. The spin coating parameters for MeO-2PACz are given in table 6.

Table 6: Spin coating parameters for MeO-2PACz.

Entry-Nr.	rpm / min^{-1}	time / s	ramp / rpm s^{-1}
1	3 000	30	1 500

For coating of the substrates with MeO-2PACz, 70 µL of the solution were dropped onto the substrates upon which the spin coating program was initiated. As soon as the substrate stopped spinning, the films were immediately transferred to a hot plate and left to anneal at 100 °C for 10 min.

As a next step the perovskite precursor solution was applied. To do this, the precursor solutions had been stirred beforehand at 65 °C for approximately 60 min. Then they had been left to cool down under stirring for approximately another 30 min upon which they were filtered through a polytetrafluoroethylene (PTFE) filter. For optimal coating a wetting agent (Methanol (MeOH), Ethanol (EtOH), 1-Propanol (1-PrOH) or 1-Butanol (1-BuOH), see **Section 3.1.2**) was used and spun onto the MeO-2PACz layer before addition of the perovskite solution. To do so, the substrates were spin coated with the program referenced in table 7. 20 s before the program

stopped 170 µL of the wetting agent were dropped onto the substrate within 1 s. As soon as the spin coating program finished, 70 µL of the perovskite precursor solution were dropped onto the wetted substrate and the spin coating program was started again immediately. As a next step, 170 µL of chlorobenzene (CB) were dropped onto the substrates as an antisolvent. This step facilitates perovskite crystal formation which was observable by an immediate colour change from yellow to brown. The antisolvent was added 35 s before the end of the spin coating program within 1 s. As soon as the spinning stopped, the perovskite films were transferred to a hot plate, where they were left to anneal at 65 °C for 2 min. Upon this they were further annealed at 100 °C for another 10 min.

Table 7: Spin coating parameters for perovskite precursor solutions.

Entry-Nr.	rpm / min^{-1}	time / s	ramp / rpm s^{-1}
1	480	1	480
2	4 000	58	2 000

2.4. Solar Cells

Upon investigation into which additive showed the best results, solar cells with these additives were fabricated analogously to the procedure described in **Section 2.3**. However, for solar cells 25 mm × 25 mm glass substrates were used, which were etched with conc. hydrochloric acid (HCl). Additionally, after applying the MeO-2PACz layer the contacts were cleaned with a cotton pad and 40 µL EtOH. The same was done after application of the perovskite layer with 40 µL of DMF. As an ETL $PC_{60}BM$ was spin coated onto the perovskite layer. For this a 20.0 mg mL^{-1} $PC_{60}BM$ solution was used, 200 µL thereof were dropped onto the perovskite upon which spin coating according to the parameters in table 8 was initiated. No eventual annealing was required for this material.

Table 8: Spin coating parameters for $PC_{60}BM$.

Entry-Nr.	rpm / min^{-1}	time / s	ramp / rpm s^{-1}
1	1 320	16	660
2	1 980	15	990

As an additional contact layer bathocuproine (BCP) was spin coated on top of the ETL. For this a 0.5 mg mL^{-1} solution of BCP was used, 200 µL thereof dropped onto the ETL and spin coating was initiated. The spin coating parameters for BCP are given in table 9. Again, after applying the BCP the contacts were cleaned with a cotton pad and 40 µL of CB.

Table 9: Spin coating parameters for BCP.

Entry-Nr.	rpm / min^{-1}	time / s	ramp / rpm s^{-1}
1	4 000	67	2 000

As the last step 100 nm of silver electrodes were evaporated onto the solar cells. This was done in an *Univex 350* thermal evaporator. This resulted in eight solar cells per substrate.

2.5. Characterization

2.5.1. PL Spectroscopy

The perovskite films were mainly investigated using PL spectroscopy. To exclude any interference from H_2O and O_2, a custom-made setup was used to keep the films under an oxygen and moisture free environment. For this, the films were encapsulated in the glove box between two glass windows and surrounded by a gasket ring. This setup was then fixated using two clamps and is depicted in Fig. 4.

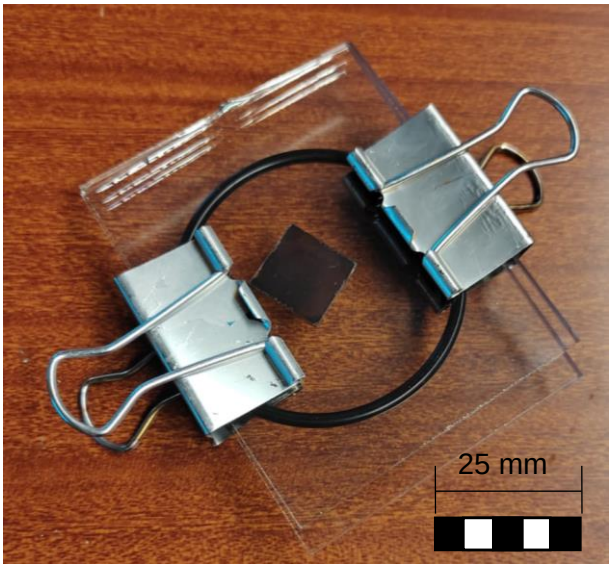

Figure 4: Encapsulation of perovskite samples.

The films were then illuminated with an *OBIS* laser diode (*coherent*) with a wavelength of 405 nm. The CCD detector used was an *iDus420* connected to a *Shamrock 303i* monochromator. The detector was cooled to -60 °C. One or two 420 nm long pass (LP) filters were used, and the signal was delivered through a glass fibre. As slit width (s.w.) and exposure time (exp) as well as laser intensity vary between the experiments, this information is given in the graphs.

2.5.2. Atomic Force Microscopy

All variations of perovskite films processed within this thesis were investigated via atomic force microscopy (AFM). The equipment used was an *Innova 2017 (Bruker)*. To qualitatively compare the different perovskite films all films were measured on a scale of 50×50 µm respectively. The scanning rate used was 50 µm s^{-1} with a resolution of 256×256 lines.

2.5.3. Scanning Electron Microscopy

The perovskite films were additionally measured by scanning electron microscopy (SEM). For this a machine of type *JSM-6360LV (Jeol)* was used. After the vacuum chamber had reached a vacuum of 10^{-4} mbar, the films were observed at a working distance (which describes the distance between lens and sample) of 12 mm at an acceleration potential of 7 kV. The samples were each investigated at a magnification factor of 500.

2.5.1. IV-Curves

The IV-characteristics of each solar cell were measured with a solar simulator of type *LOT-Quantum Design* using a xenon arc lamp with filter. Here the voltage was swept from -1 to 1.5 V and the resulting current was measured using a *Keithley 2041 Source Meter*. For calibration a silicon solar cell of type *Si-01TC* (*Mencke&Tegtmeyer)* was used. Additionally, the IV curves of all solar cells were also measured every minute for a duration of 10 min to investigate losses over an extended period of continuous illumination.

2.5.2. External Quantum Efficiency

External Quantum Efficiency (EQE) measurements were performed in a glove box atmosphere with a setup of type *LXH 100 (Müller)*, a *SpectraPro-150 (Acton)* monochromator and a lock-in amplifier of type *7260 DSP (EG&G Instruments)*. A silicon photodiode of type *Hamamatsu S2281* was used for calibration.

3. Results & Discussion

3.1. Perovskite Films

3.1.1. Variation of Bromide Concentration

As a first step, the behaviour of the resulting photoluminescence in relationship with different bromide contents of the perovskite films was investigated. For this, films with the compositions $FA_{0.8}Cs_{0.2}PbI_3$, $FA_{0.8}Cs_{0.2}Pb(I_{0.8}Br_{0.2})_3$ as well as $FA_{0.8}Cs_{0.2}Pb(I_{0.6}Br_{0.4})_3$ were fabricated according to the procedure given in **Section 2.2**. As expected [10,16,17], the signal shifted towards shorter wavelengths with increase in bromide concentration. The films were constantly illuminated for 10 min, after which the formation of a shoulder could already be observed. Upon illumination the films were left in the dark for additional 10 min before they were measured again. This resulted in a disappearance of the shoulder and a partial return to the original state, as can be seen in Fig. 5. It could also be observed that the degradation of the film and hence the appearance of the shoulder happened quicker for higher bromide concentrations.

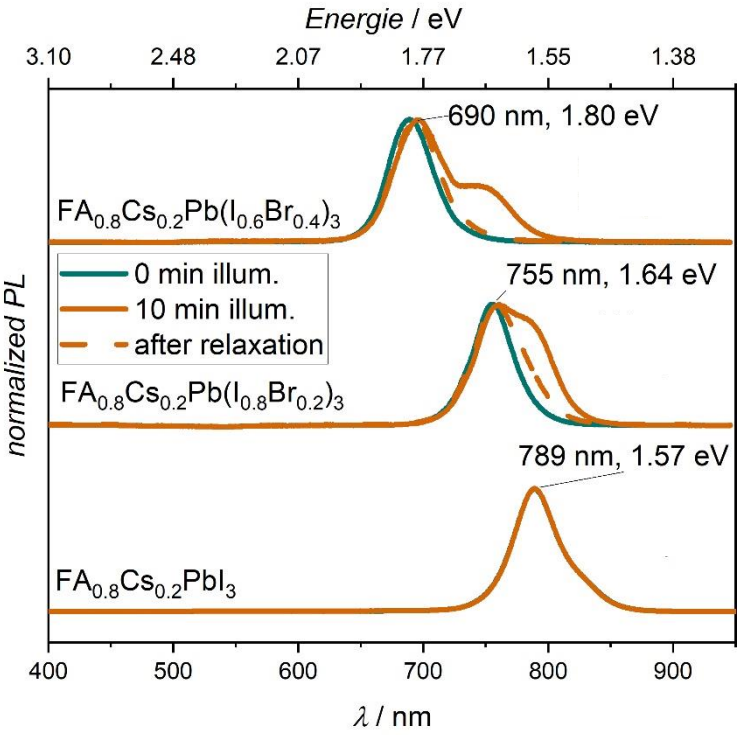

Figure 5: Phase segregation in perovskite films with composition $FA_{0.8}Cs_{0.2}PbI_3$ (100 µm s.w., 1 s exp), $FA_{0.8}Cs_{0.2}Pb(I_{0.8}Br_{0.2})_3$ (200 µm s.w., 2 s exp) and $FA_{0.8}Cs_{0.2}Pb(I_{0.6}Br_{0.4})_3$. (200 µm s.w., 2 s exp) Laser intensity 1.71 mW.

3.1.2. Variation of Wetting Agent

As the perovskite is reported [29] to grow more favourably on the HTL after treating the HTL with a wetting agent, it was investigated, which wetting agent would result in the perovskite structure with the least shoulder formation. For this MeOH, EtOH, 1-PrOH as well as 1-BuOH were used and compared to samples that had undergone no wetting at all. It was already observable by eye that wetting clearly improved the crystal structure formation when compared to not wetting them, as is depicted in Fig. 6.

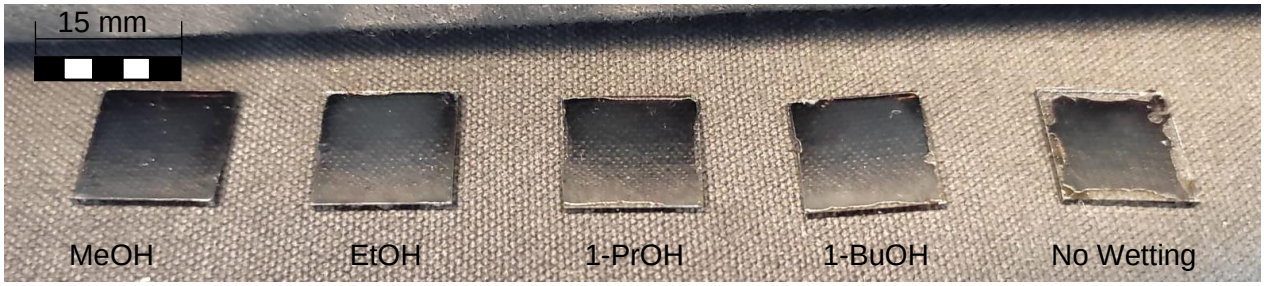

Figure 6: Comparison of perovskite films with different wetting agents.

Of these films PL-spectra were recorded as well. The films with 1-BuOH and without any wetting agent showed the strongest phase segregation after 10 min of illumination, as is visible in Fig. 7a. On the other hand, 1-PrOH, EtOH and MeOH showed comparable results in suppression of phase segregation. As wetting with MeOH also resulted in a large grain size, as observable in Fig. 8 and 9, it was further used as wetting agent unless stated differently.

To investigate whether the occurring phase segregation is dependent on residual solvent present in the perovskite films, the films were transferred to a vacuum chamber for 2 h. The pressure had been 10^{-5} mbar at the beginning and had gone down to 9×10^{-7} mbar towards the end. However, no noticeable difference could be observed upon vacuum treatment of the films, as shown in Fig. 7b. Additionally, both AFM scans and SEM images were performed with the perovskite films. The results can be seen in Fig. 8 and 9.

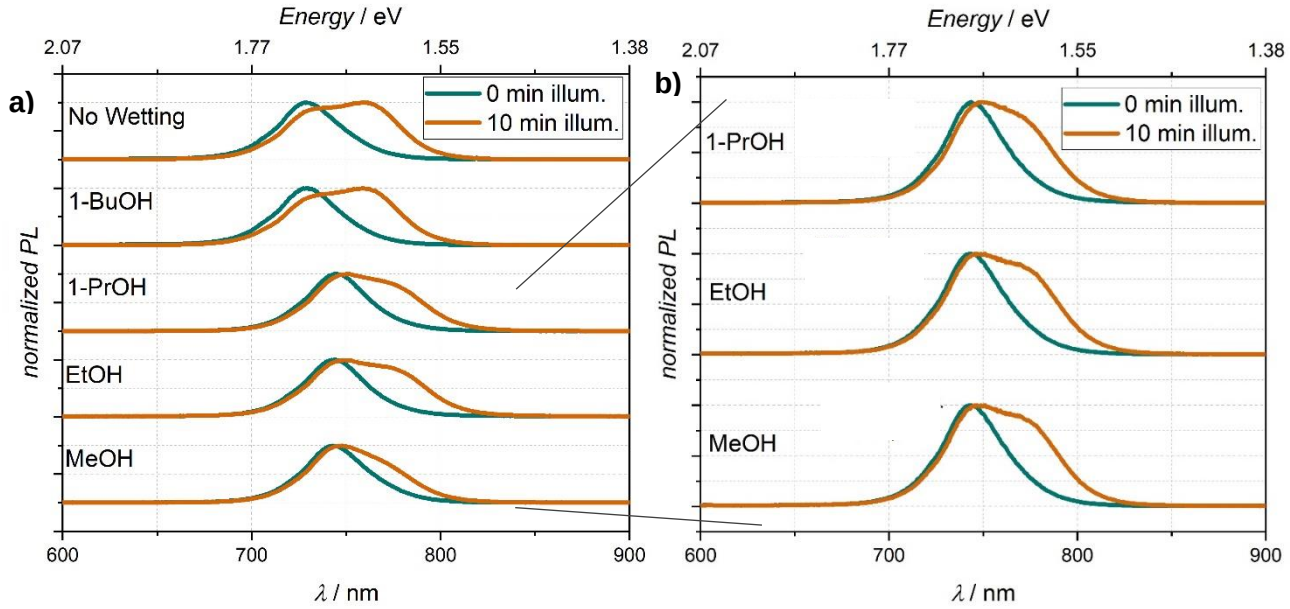

Figure 7: a) Phase segregation in $FA_{0.8}Cs_{0.2}Pb(I_{0.8}Br_{0.2})_3$ perovskite films with comparison of different wetting agents. Measurement conditions were 100 µm s.w., 1 s exp for 1-PrOH, 1-BuOH and no wetting and 200 µm, 2 s exp for MeOH and EtOH b) Phase segregation in same perovskite films after vacuum treatment. Measurement conditions were 150 µm s.w., 1.5 s expfor EtOH and 1-PrOH and 100 µm s.w., 1 s exp for MeOH Laser intensity 1.84 mW.

3.1.3. SEM and AFM of Wetting Agents

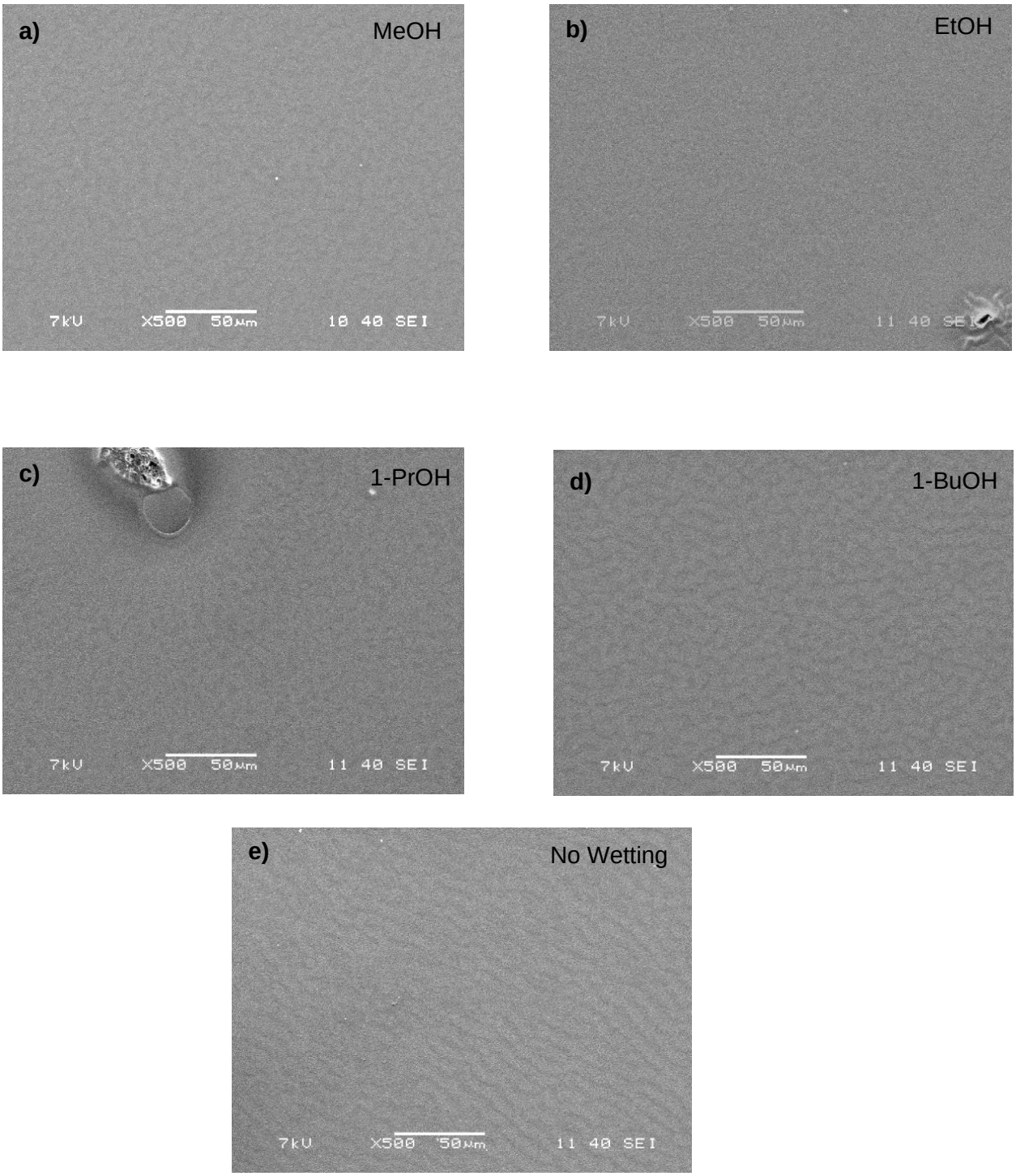

Figure 8: SEM scans of $FA_{0.8}Cs_{0.2}Pb(I_{0.8}Br_{0.2})_3$ perovskite films with different wetting agents at a magnification factor of 500. a) MeOH, b) EtOH,c) 1-PrOH, d) 1-BuOH and e) without wetting.

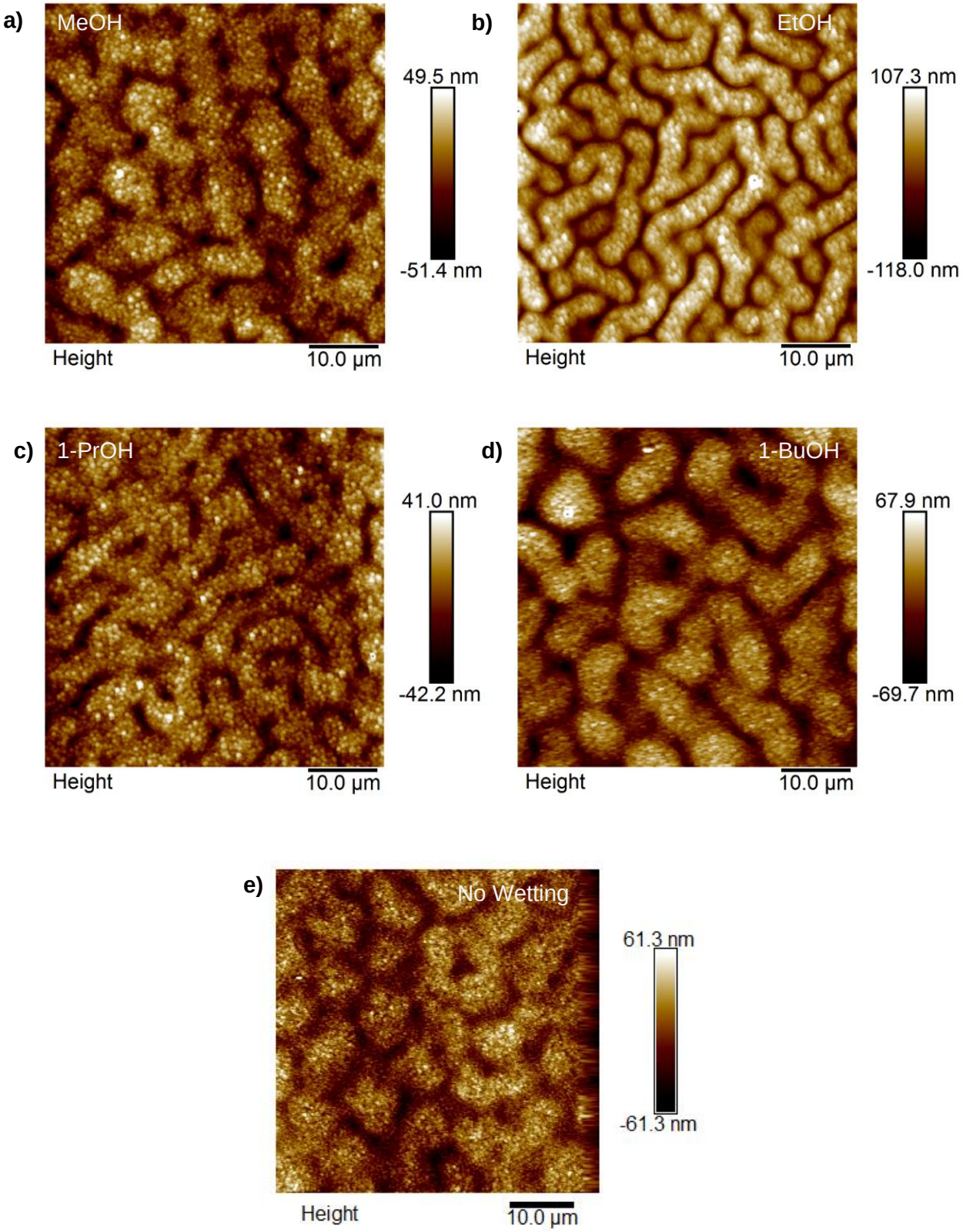

Figure 9: AFM scans of $FA_{0.8}Cs_{0.2}Pb(I_{0.8}Br_{0.2})_3$ perovskite films with different wetting agents at a scale of 50×50 µm. a) MeOH, b) EtOH,c) 1-PrOH, d) 1-BuOH and e) without wetting.

3.1.4. Illumination/Relaxation Cycles

As a next step the reversibility of the phase segregation was investigated. To do so, a perovskite film of composition $FA_{0.8}Cs_{0.2}Pb(I_{0.8}Br_{0.2})_3$ was illuminated in cycles of 10 min of continuous illumination (Fig. 10a) with 10 min of relaxation in complete darkness (Fig. 10b) for four times each.

Not only could it be observed from these spectra that the maximum shifted towards higher wavelengths, but it could also be seen that the maximum increased in PL-count intensity with each cycle of illumination. This might be an indication for a degradation process as postulated by Stoddard, et al. [31], who found that the perovskite PL-signal increased upon light-induced decomposition. The initial increase here might be due to carrier localization in the illuminated region. The eventual decrease is postulated to occur due to degradation of the perovskite material into PbI_2 domains.

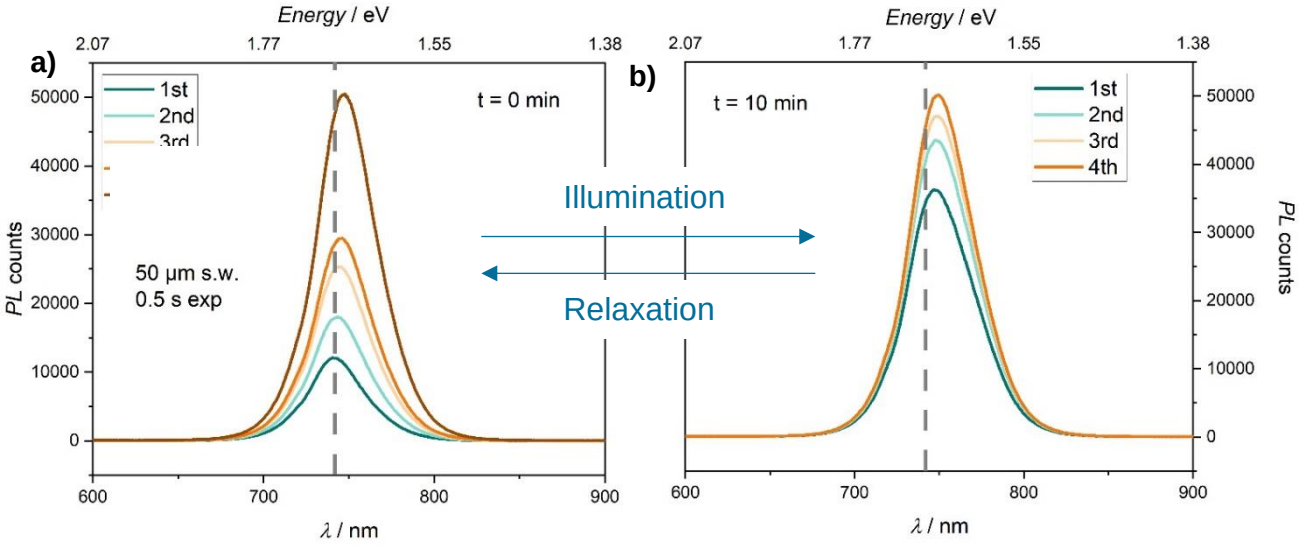

Figure 10: PL spectra of continuous illumination cycles a) after relaxation, b) after illumination. The dotted line represents the maximum of the initial state. Measurement conditions were 50 µm s.w., 0.5 s exp Laser intensity 4.02 mW.

3.1.5. Continuous Illumination for 6.5 h

As a next step it was investigated whether a saturation in peak intensity could be found. For this, a perovskite film of composition $FA_{0.8}Cs_{0.2}Pb(I_{0.6}Br_{0.4})_3$ was illuminated constantly over a period of 6.5 h.

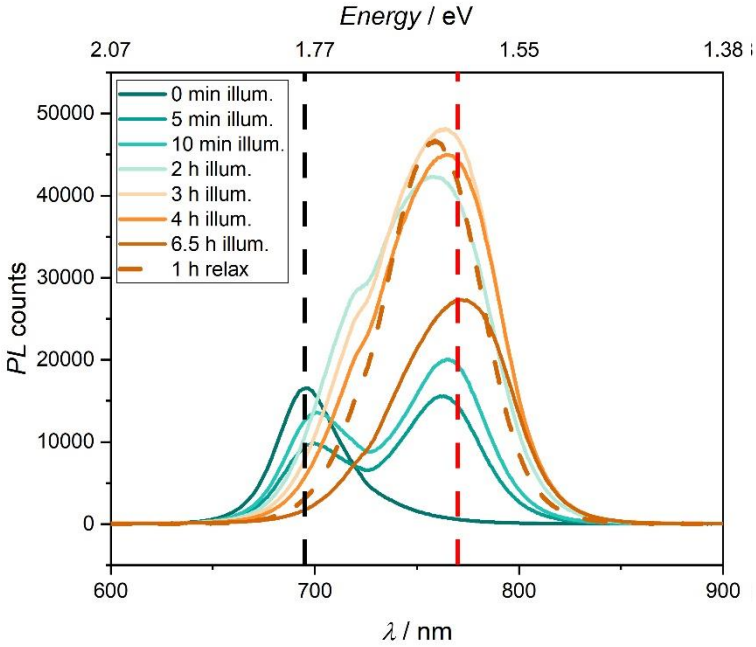

Figure 11: Constant illumination of a $FA_{0.8}Cs_{0.2}Pb(I_{0.6}Br_{0.4})_3$ perovskite film for 6.5 h. The black dotted line represents the maximum at the initial state, whereas the red dotted line represents the maximum of the saturated state. Measurement conditions were 50 µm s.w., 0.5 s exp. Laser intensity 4.28 mW.

As can be seen in Fig. 11, phase segregation in a perovskite film with 40% bromide content already starts to occur after a few minutes. Also it can be seen that the PL-signal increased in intensity upon illumination as was the case in **Section 3.1.4**. However, the signal then decreased in intensity again after about 4 h of constant illumination, until it reached a saturation intensity after about 5 h. Interestingly, upon 1 h of relaxation in complete darkness, the peak did not return to its original maximum at 695 nm, but was much closer to the wavelength at saturation (770 nm). This might be an indication that the reversibility postulated [16] might not be given anymore once the perovskite film has advanced in decomposition. Also after relaxation the peak increased again in intensity.

The fitting of the curves was done by fitting each individual peak as depicted in Fig. 12. By combining them, the cumulative peak then approaches the obtained signal. To deduct information about the impact of the phase segregation, the share of the peak area of each individual peak (A_x) in percent of the total peak area (A) is plotted against time.

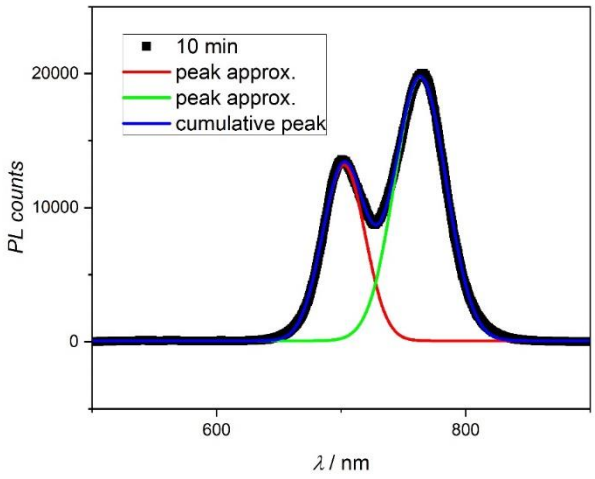

Figure 12: Fitting example of PL-curves.

The relation between the areas under both peaks is given as a percentage in Fig. 13. As can be seen, after 1.5 h already 90% of the combined peak area can be attributed to the peak emerging at 770 nm, indicating a rapid degradation of the perovskite film.

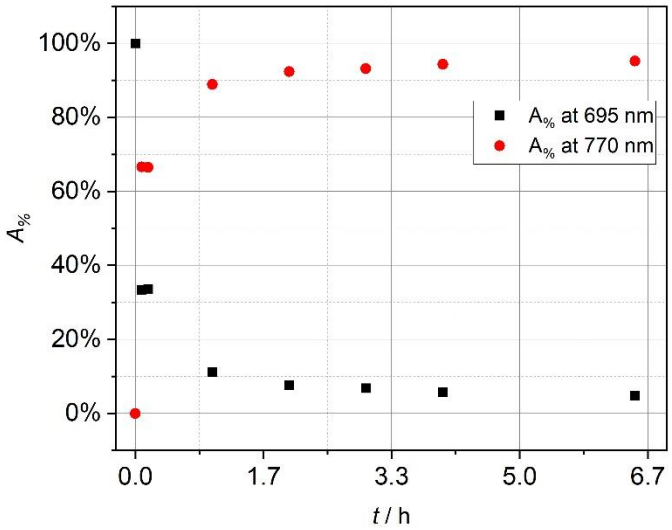

Figure 13: Share of peak areas at 695 nm and 770 nm respectively.

3.2. Additives

3.2.1. Potassium Iodide

As a first additive KI was investigated. As visible in Fig. 14a, in the case of the pristine perovskite film used as reference a shoulder formed after 10 min of continuous illumination. However, in the case of the film with KI used as an additive, not only did a shoulder form, but merely a second peak emerged after only 10 min of illumination. It could not be observed within this thesis that KI could successfully suppress the phase segregation, therefore no further experiments with KI were performed.

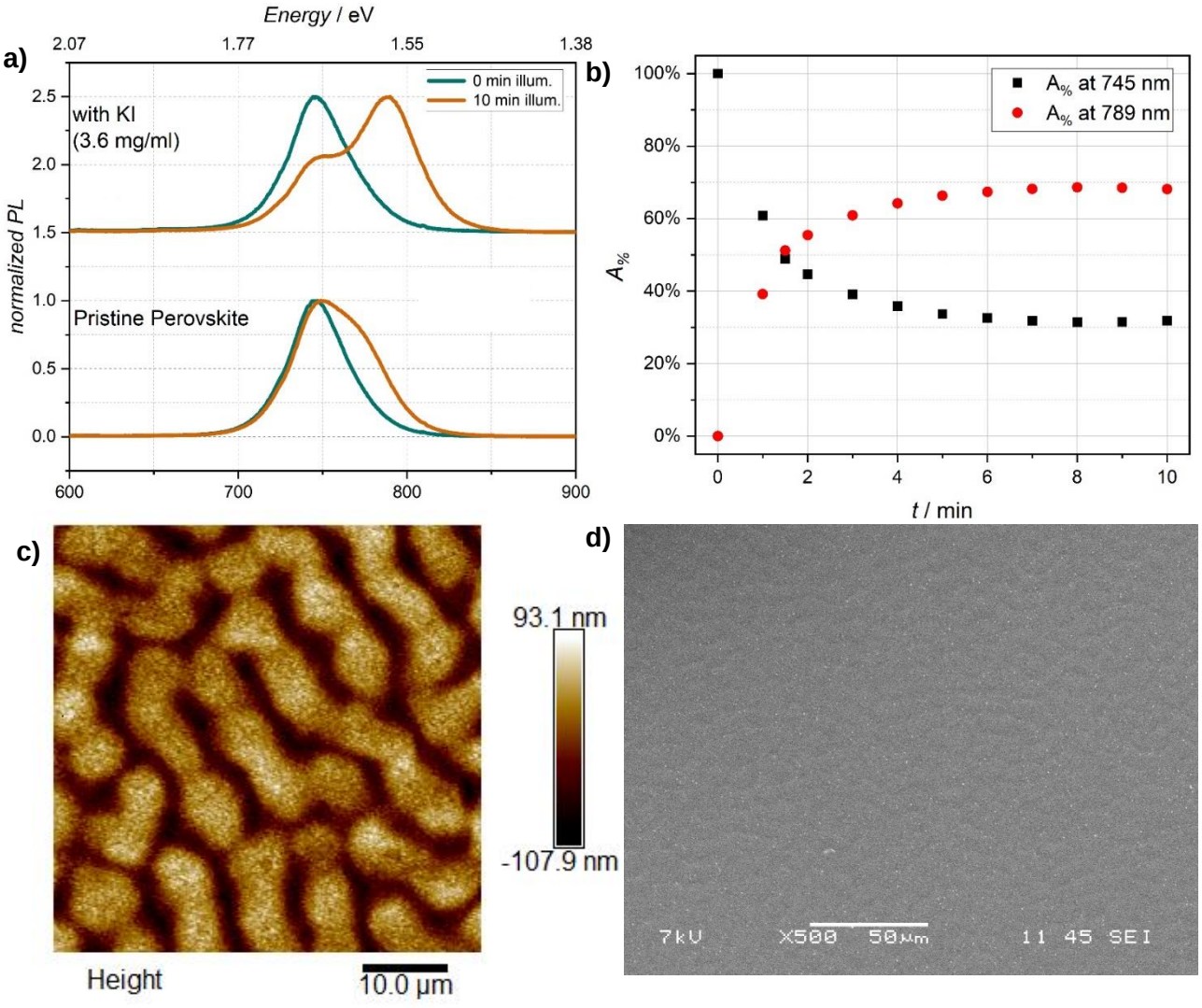

Figure 14: a) Phase segregation in $FA_{0.8}Cs_{0.2}Pb(I_{0.8}Br_{0.2})_3$ perovskite films with 3.6 mg mL^{-1} KI with laser intensity 1.41 mW, measurement conditions were 100 µm s.w., 1 s exp. b) share of peak areas at 745 nm and 789 nm respectively, c) AFM image, d) SEM image.

3.2.2. Phenethyl ammonium iodide

Although some sources indicate application of the PEAI from solution onto the processed perovskite films [27], in this thesis the PEAI was added to the precursor solution like described in literature [17,28]. For this a perovskite precursor solution was used with PEAI added according to **Section 2.2**. The films were processed according to standard procedure and investigated with the PL-setup. Contrary to the KI-films, the PEAI-films did not segregate. However, the initial peak entirely moved towards higher wavelengths. The behaviour of both, the peak maximum as well as the peak area over time, are depicted in Fig. 15.

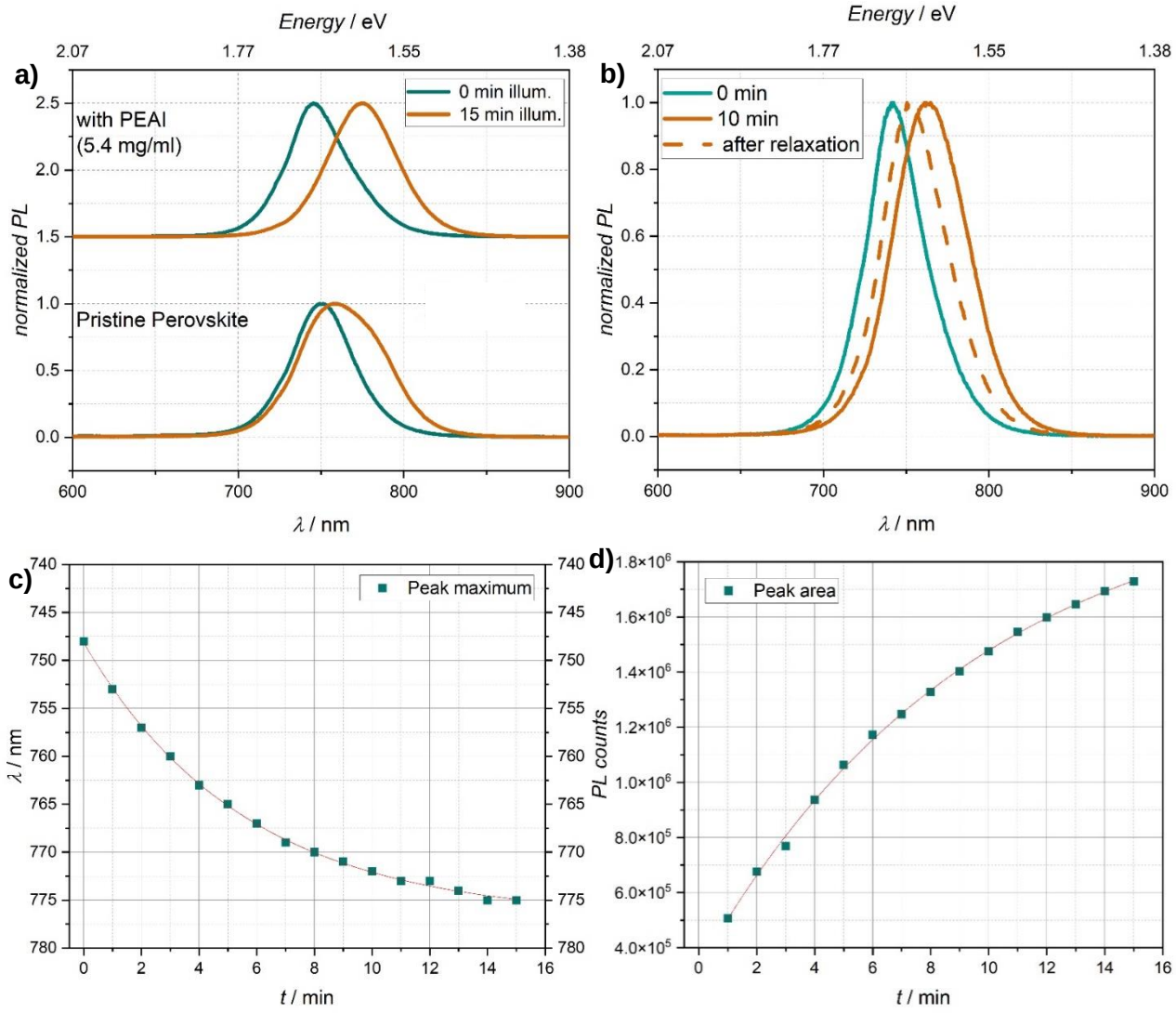

Figure 15: a) Behaviour of $FA_{0.8}Cs_{0.2}Pb(I_{0.8}Br_{0.2})_3$ upon illumination, measurement conditions were 100 µm s.w., 1 s exp. b) effect of relaxation on same film, c) position of peak maximum over time, d) peak area over time.

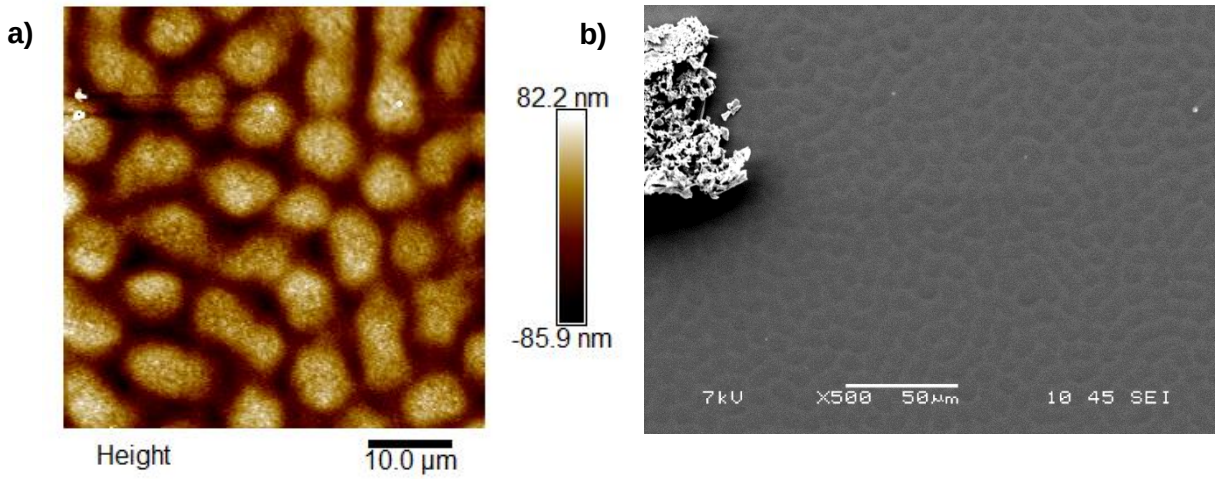

Figure 16: a) AFM of $FA_{0.8}Cs_{0.2}Pb(I_{0.8}Br_{0.2})_3$ perovskite films with 8.1 mg mL^{-1} PEAI, b) SEM image.

3.2.3. Lead Thiocyanate

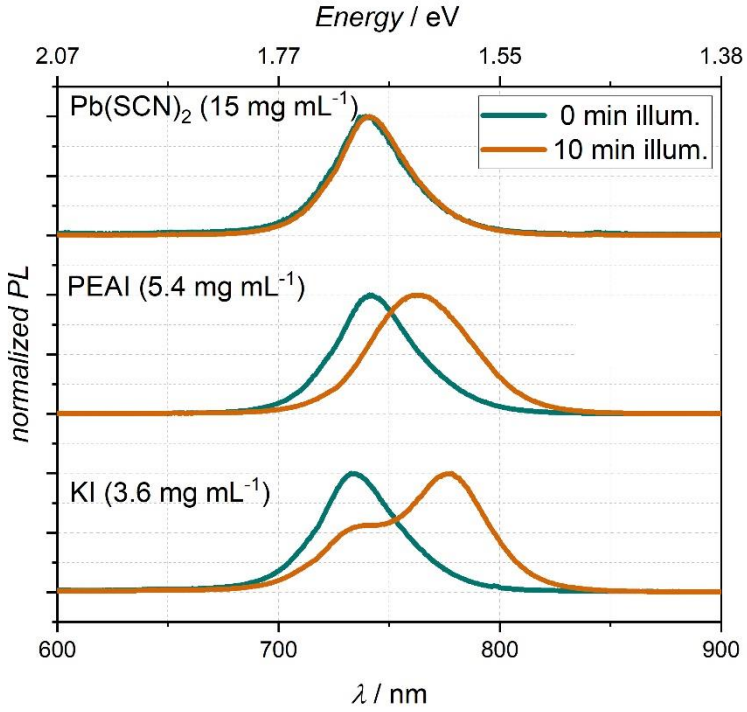

Figure 17: Comparison of phase segregation in $FA_{0.8}Cs_{0.2}Pb(I_{0.8}Br_{0.2})_3$ perovskite films with KI, PEAI and $Pb(SCN)_2$. Measurement conditions were 100 µm s.w., 1 s exp. Laser intensity 2.08 mW.

As a last additive $Pb(SCN)_2$ was observed. As can be seen in Fig. 17, $Pb(SCN)_2$ showed the most promising results within the scope of this thesis and was thus further investigated.

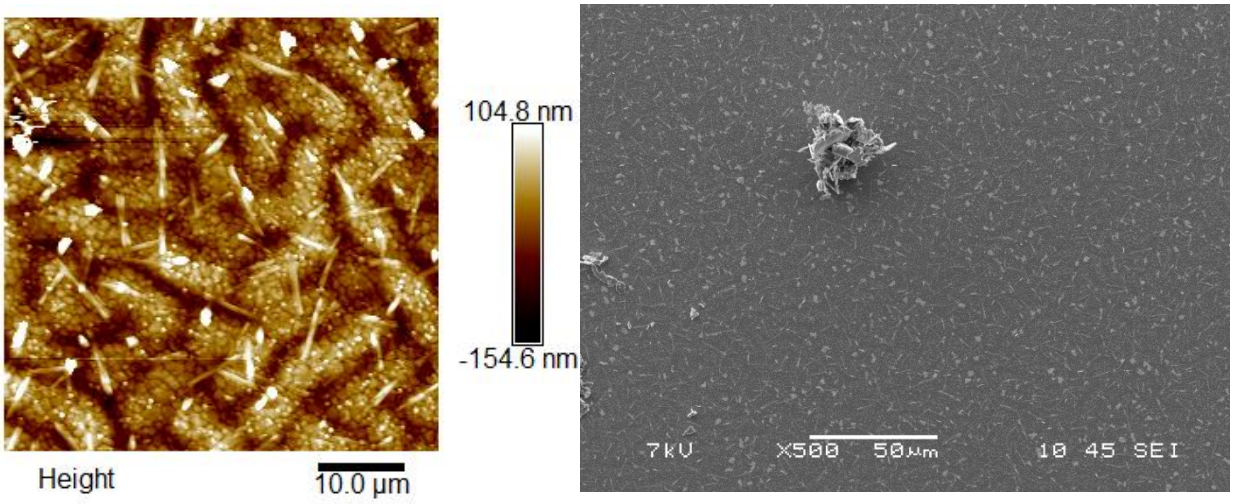

Figure 18: a) AFM of $FA_{0.8}Cs_{0.2}Pb(I_{0.8}Br_{0.2})_3$ perovskite films with 15.0 mg mL^{-1} $Pb(SCN)_2$, b) SEM image.

Contrary to the other additives, upon adding $Pb(SCN)_2$ to the perovskite, not only were the grain boundaries more pronounced, but also needle-like structures formed on a microscopic scale as clearly visible in the AFM scan displayed in Fig. 18a.

As a next step the bromide concentration of $Pb(SCN)_2$ perovskite films was increased. When moving to a bromide concentration of 40%, the films with the additive degraded even faster, than the pristine $FA_{0.8}Cs_{0.2}Pb(I_{0.6}Br_{0.4})_3$ film. This can be seen in Fig. 19, where the share of the peak area of the peak emerging at 790 nm is plotted against time.

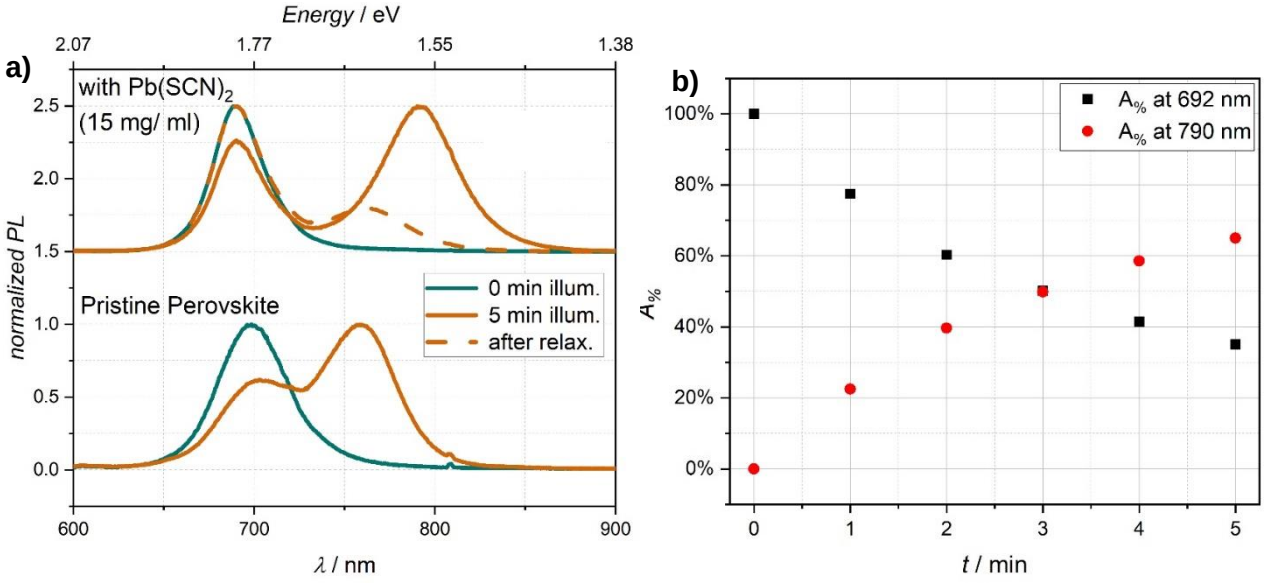

Figure 19: a) Phase segregation in PL-spectrum of $FA_{0.8}Cs_{0.2}Pb(I_{0.6}Br_{0.4})_3$ perovskite films, b) share of peak area at 692 nm and 790 nm respectively for films with $Pb(SCN)_2$, c) share of peak area at 790 nm for different concentrations of $Pb(SCN)_2$. Measurement conditions were 50 µm s.w., 0.5 s exp. Laser intensity 1.58 mW.

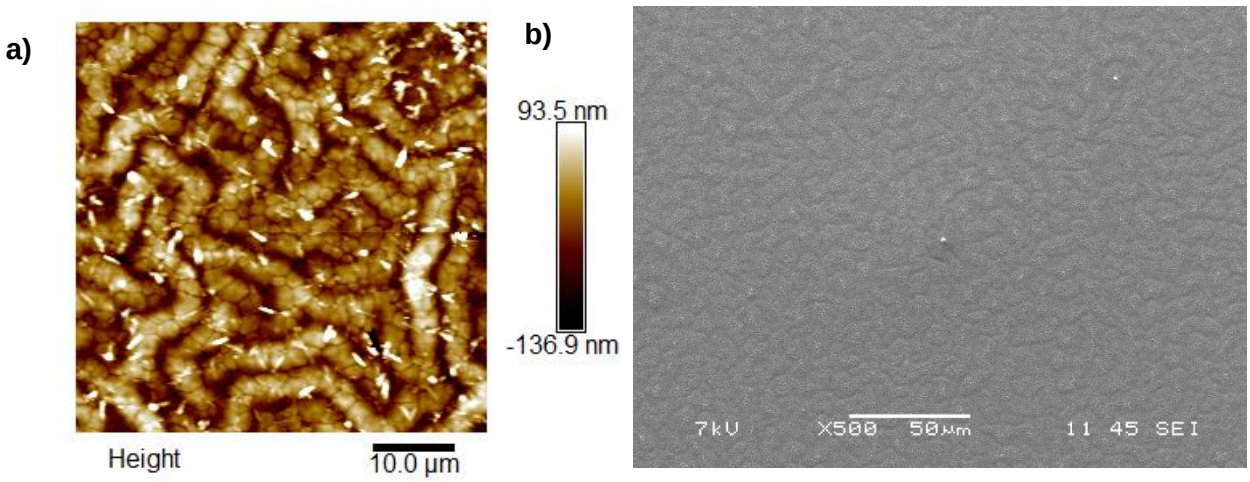

Figure 20: a) AFM of $FA_{0.8}Cs_{0.2}Pb(I_{0.6}Br_{0.4})_3$ perovskite films with 15.0 mg mL^{-1} $Pb(SCN)_2$, b) SEM image.

Again, as it was the case with the $FA_{0.8}Cs_{0.2}Pb(I_{0.8}Br_{0.2})_3$ films, also here the formation of needles can be seen. Furthermore, using a $FA_{0.8}Cs_{0.2}Pb(I_{0.6}Br_{0.4})_3$ film with $Pb(SCN)_2$ added as an additive the grain size increased. This is best visible in Fig. 20a.

To investigate, whether a different additive concentration resulted in more stable films, the $Pb(SCN)_2$ concentration was varied. However, all attempts with different concentrations of the additive also degraded faster, than the films measured with a $Pb(SCN)_2$ concentration of 15 mg mL^{-1}, as visible in Fig. 21. Therefore, it is likely that this is due to minor variations during the fabrication such as the glovebox atmosphere.

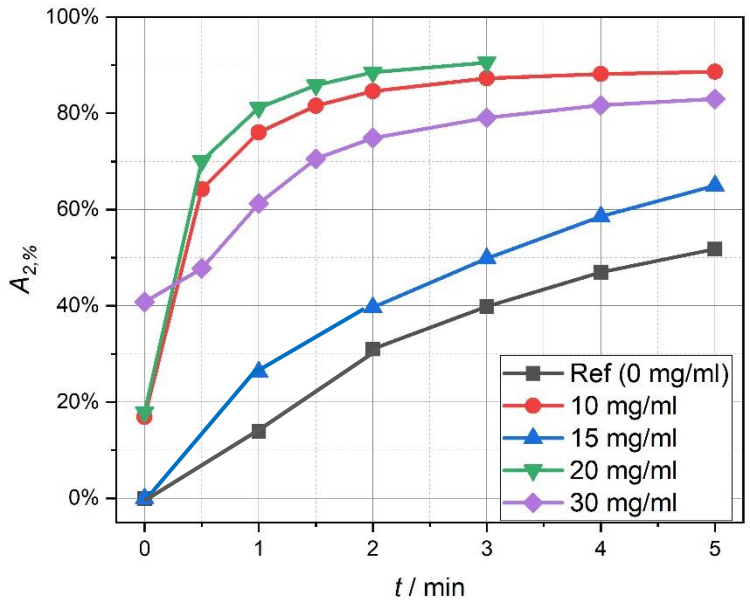

Figure 21: Share of peak area for $FA_{0.8}Cs_{0.2}Pb(I_{0.6}Br_{0.4})_3$ perovskite films at 790 nm for different concentrations of $Pb(SCN)_2$.

3.3. Solar Cells

Upon the investigations of **Section 3.1** and **3.2** considering the additives, solar cells were produced according to the procedure described in **Section 2.4**. For this, PSCs of composition $FA_{0.8}Cs_{0.2}Pb(I_{0.8}Br_{0.2})_3$ as well as $FA_{0.8}Cs_{0.2}Pb(I_{0.6}Br_{0.4})_3$ both with and without 15 mg mL^{-1} of $Pb(SCN)_2$ were fabricated. The solar cells were then analysed in terms of IV measurements, PL-spectroscopy and EQE determination.

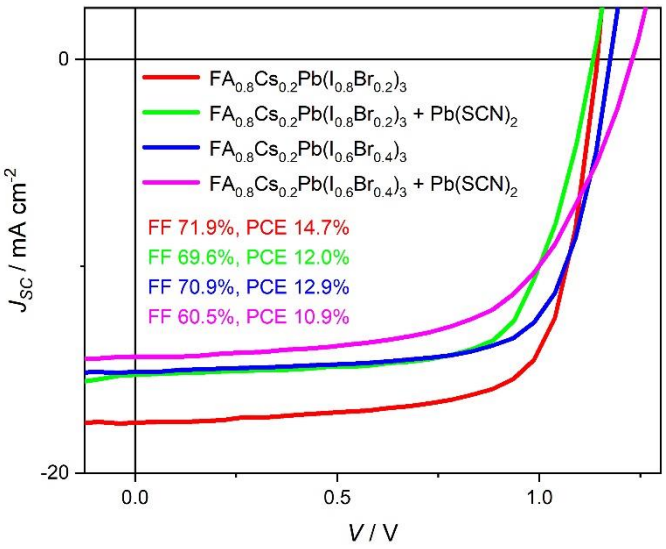

Figure 22: IV-curves of best performing solar cells of each type.

3.3.1. IV-Curves

The IV-curve of the best performing solar cells of each type are shown in Fig. 22. As visible not only did the solar cells without additives perform better in terms of FF as well as PCE than their $Pb(SCN)_2$ counterparts, A statistical overview about the performance of all solar cells is depicted in Fig. 23 as well as in table 10.

Table 10: Performance of each solar cell type.

Composition	V_{OC} / V	J_{SC} / mA cm^{-2}	FF / %	PCE / %	n
$FA_{0.8}Cs_{0.2}Pb(I_{0.8}Br_{0.2})_3$	1.15	19.1	72	14.7	22
	(1.09 ± 0.06)	(17.5 ± 1.1)	(64 ± 6)	(12.2 ±1.6)	
$FA_{0.8}Cs_{0.2}Pb(I_{0.8}Br_{0.2})_3$	1.13	17.9	70	12.0	7
+ $Pb(SCN)_2$	(1.05 ± 0.04)	(17.1 ± 1.0)	(60 ± 5)	(10.7 ± 0.7)	
$FA_{0.8}Cs_{0.2}Pb(I_{0.6}Br_{0.4})_3$	1.21	15.4	71	12.9	14
	(1.13 ± 0.09)	(13.3 ± 1.5)	(53 ± 17)	(8.4 ± 3.3)	
$FA_{0.8}Cs_{0.2}Pb(I_{0.6}Br_{0.4})_3$	1.09	15.2	61	10.9	14
+ $Pb(SCN)_2$	(0.90 ± 0.09)	(13.7 ± 1.4)	(50 ± 8)	(6.2 ± 1.5)	

As can be seen from the statistical data in table 10 that V_{OC} increases upon increasing the band gap. This is inspected upon increasing the perovskites bromide concentration. It was also found that the J_{SC} decreased upon increase of the band gap.

However, it was found that solar cell performance decreased immediately once the cells were illuminated for some time. For each solar cell a measurement was taken, where the cells were continuously exposed to light for a duration of 10 min and the resulting IV-curves were recorded. The respective IV-curves of each solar cell are given in Fig. 25. As can be seen, for all solar cells the J_{SC} decreased upon illumination. This might be due to the occurring phase segregation. Noticeably, all solar cells showed worse performance after continuous illumination, however, in the case of $FA_{0.8}Cs_{0.2}Pb(I_{0.8}Br_{0.2})_3$ without any additive, it appears that the solar cell PCE increased after 10 min. On the other hand, this result could not be reproduced, and repeated measurements showed the same trend as all other solar cells.

The resulting decrease in PCE with time is graphically represented in Fig. 24. Although the PCE decreased in all solar cells upon illumination, this was particularly drastic for the solar cells with a higher band gap. As can be seen the PCE decrease in the $FA_{0.8}Cs_{0.2}Pb(I_{0.8}Br_{0.2})_3$ with and without $Pb(SCN)_2$ as an additive was only 6.7% (pristine) and 13.6% (additive) compared to the initial PCE respectively. However, in the case of PSCs with a composition of $FA_{0.8}Cs_{0.2}Pb(I_{0.6}Br_{0.4})_3$ a tremendous decrease of 54.7% (pristine) and 44.0% (additive) could be measured. This correlates to the faster occurrence of the phase segregation effect as visible when comparing Fig. 17 and Fig 19a.

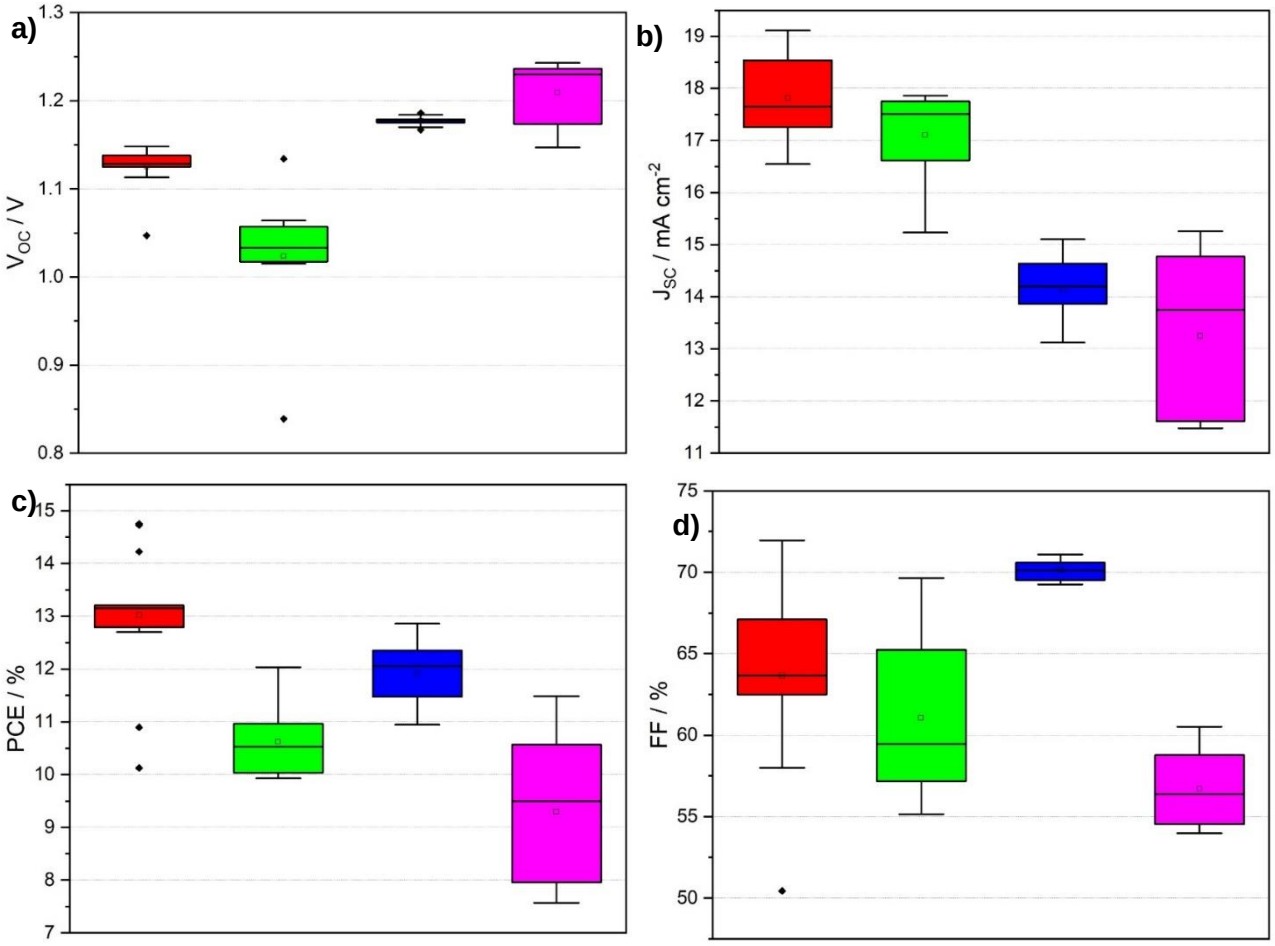

Figure 23: Boxplot of performance of each type of solar cell a) V_{OC}, b) J_{SC}, c) PCE and d) FF. $FA_{0.8}Cs_{0.2}Pb(I_{0.8}Br_{0.2})_3$, $FA_{0.8}Cs_{0.2}Pb(I_{0.8}Br_{0.2})_3$ with $Pb(SCN)_2$, $FA_{0.8}Cs_{0.2}Pb(I_{0.6}Br_{0.4})_3$ and $FA_{0.8}Cs_{0.2}Pb(I_{0.6}Br_{0.4})_3$ with $Pb(SCN)_2$.

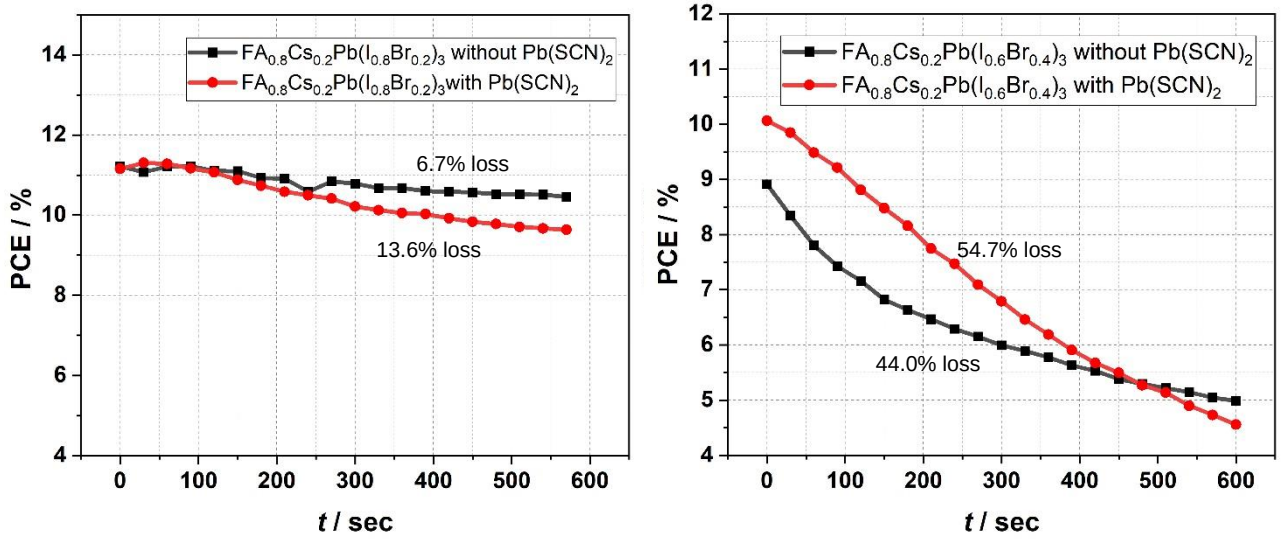

Figure 24: PCE of all solar cells over time a) $FA_{0.8}Cs_{0.2}Pb(I_{0.8}Br_{0.2})_3$ and b) $FA_{0.8}Cs_{0.2}Pb(I_{0.6}Br_{0.4})_3$.

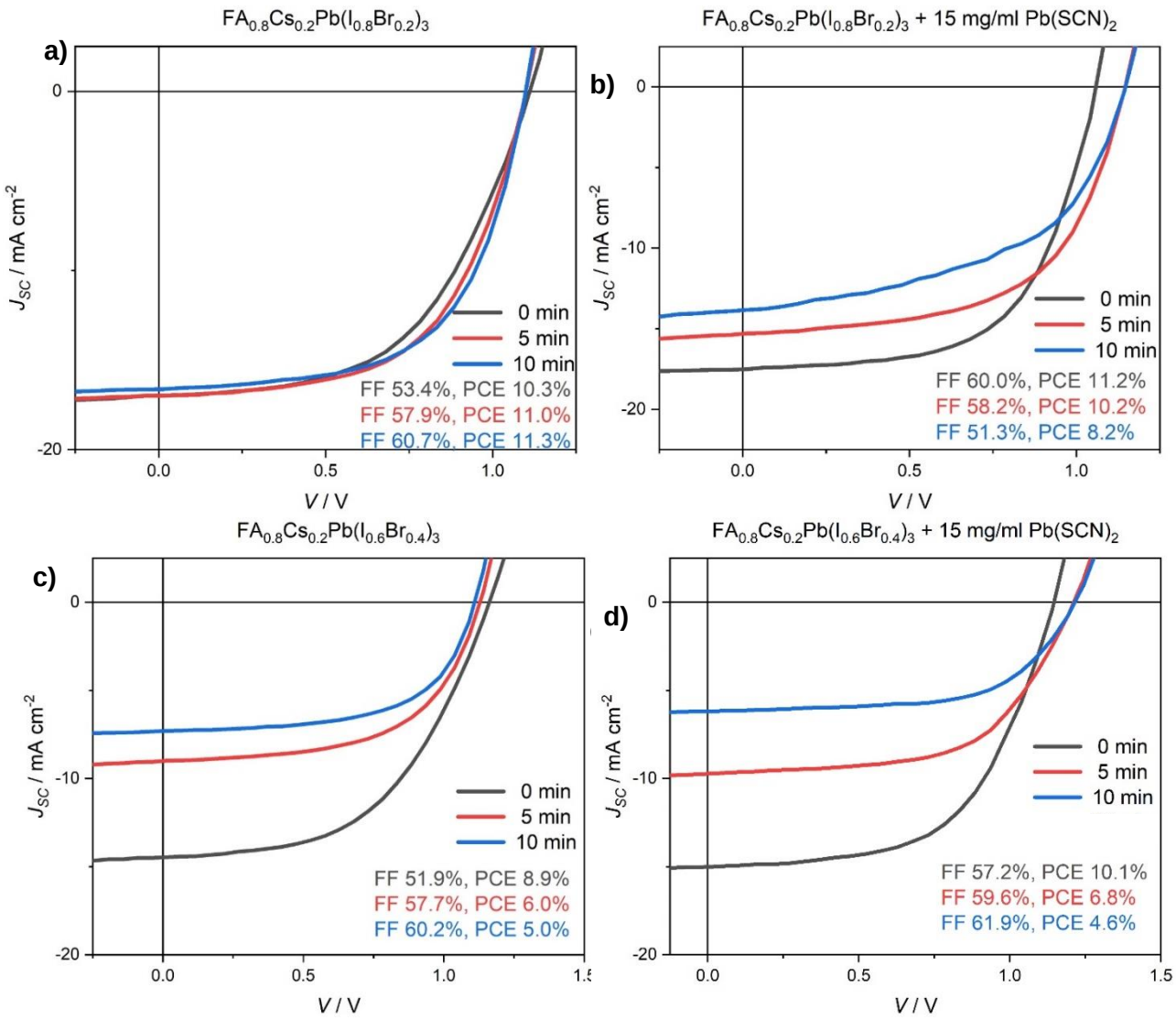

Figure 25: IV-curves of all solar cells and their decrease in performance over time a) $FA_{0.8}Cs_{0.2}Pb(I_{0.8}Br_{0.2})_3$, b) $FA_{0.8}Cs_{0.2}Pb(I_{0.8}Br_{0.2})_3$ with $Pb(SCN)_2$, c) $FA_{0.8}Cs_{0.2}Pb(I_{0.6}Br_{0.4})_3$ and d) $FA_{0.8}Cs_{0.2}Pb(I_{0.6}Br_{0.4})_3$ with $Pb(SCN)_2$.

3.3.2. PL Measurements

The solar cells were observed with a PL-setup to further investigate the phase segregation within their perovskite core. Due to the encapsulation all probes of the $FA_{0.8}Cs_{0.2}Pb(I_{0.8}Br_{0.2})_3$ with $Pb(SCN)_2$ were destroyed, that is why only PL-spectra as well as EQE-curves of the other three types exist. The spectrum for the pristine $FA_{0.8}Cs_{0.2}Pb(I_{0.8}Br_{0.2})_3$ cell is depicted in Fig. 26a, whereas the spectra of both types of $FA_{0.8}Cs_{0.2}Pb(I_{0.6}Br_{0.4})_3$ cells are shown in Fig. 26b,c.

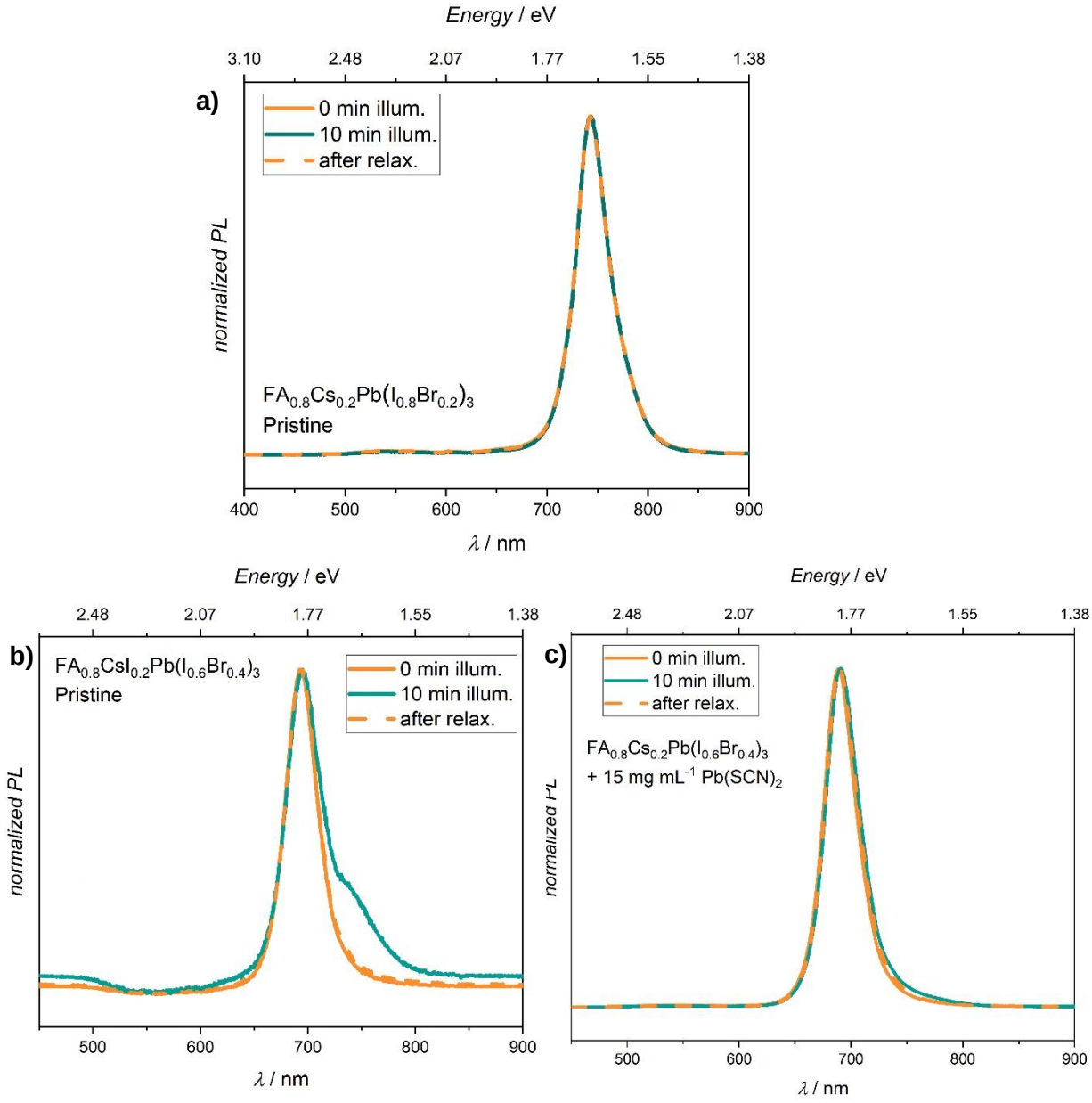

Figure 26: Comparison of phase segregation in a) $FA_{0.8}Cs_{0.2}Pb(I_{0.8}Br_{0.2})_3$ perovskite solar cells (100 µm s.w., 1 s exp), b) $FA_{0.8}Cs_{0.2}Pb(I_{0.6}Br_{0.4})_3$ cells and c) $FA_{0.8}Cs_{0.2}Pb(I_{0.6}Br_{0.4})_3$ cells with $Pb(SCN)_2$ (200 µm s.w., 2 s exp each). Laser intensity 1.90 mW.

For the pristine perovskite cell with a 20% bromide content almost no phase segregation occurs, the same is true for the 40% bromide cell with the additive. In the case of the pristine 40% bromide cell however, the formation of a shoulder can still be observed. The suppression of the phase segregation can be attributed to the passivating effect of the $PC_{60}BM$ layer that was not used in **Section 3.2**. This does however not explain, why both J_{SC} as well as PCE decreased that drastically in the IV-curves of the respective $FA_{0.8}Cs_{0.2}Pb(I_{0.6}Br_{0.4})_3$ solar cells.

3.3.3. EQE

It was discovered that by encapsulating the solar cells with the epoxy resin used, the cells were destroyed completely. That is why a glovebox-intern EQE-setup was used as described in **Section 2.5.2**. The EQE was then plotted as a Tauc-plot, where $(\alpha \times E)^2$ is plotted against the energy. However, the form of a "quasi-Tauc" plot was used. Here $(EQE \times E)^2$ is graphically depicted against the energy and the band gap can be determined by extrapolating the linear regime of each curve to the abscissa [32]. The expectation that PSCs, which show a higher bromide content also have a larger bandgap is supported by the results. It was found that the $FA_{0.8}Cs_{0.2}Pb(I_{0.6}Br_{0.4})_3$ cells had a band gap of 1.63 eV, whereas the $FA_{0.8}Cs_{0.2}Pb(I_{0.8}Br_{0.2})_3$ cells (with and without additive) showed a band gap of 1.78 eV. Both the EQE curves as well as the "quasi-Tauc" plot can be seen in Fig. 27.

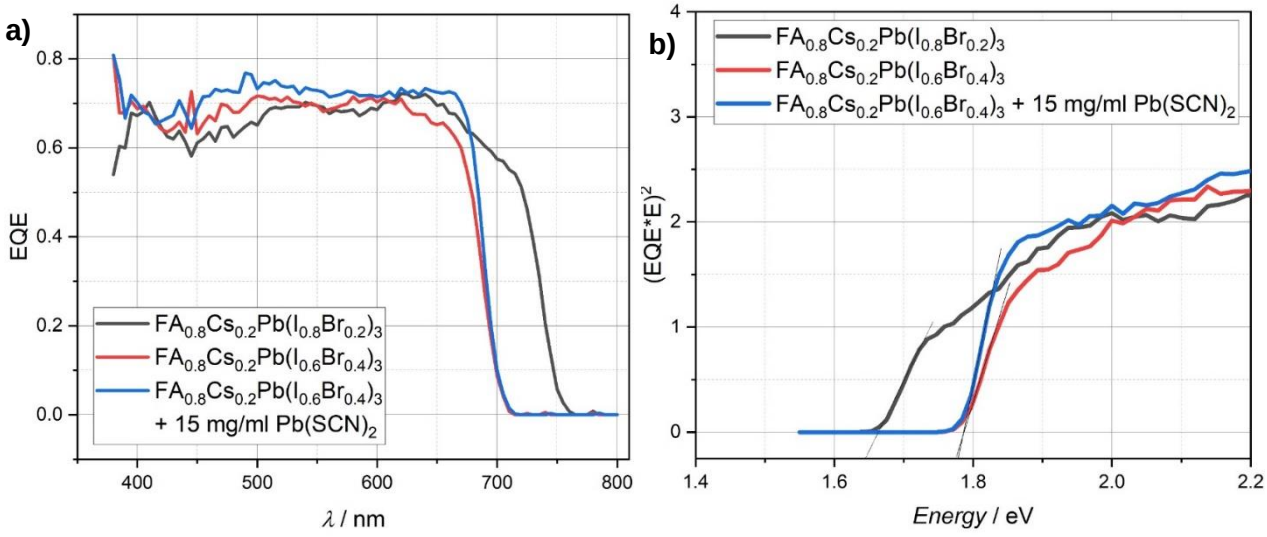

Figure 27: a) EQE curves of perovskite solar cells, b) "quasi-Tauc" plot of perovskite solar cells with determined band gap.

4. Conclusion

In the scope of this thesis the phase segregation (Hoke-effect) was investigated further and KI, PEAI as well as $Pb(SCN)_2$ were studied as additives to suppress this segregation. However, none of the additives could fully suppress the phase segregation and moving towards higher bromide content in perovskites and thus creating a larger band gap remains a challenge. By measuring the EQE of the processed solar cells and by investigating the PL-behaviour of the perovskite films it could be shown that the band gap of perovskites increases with a higher bromide ratio. Also, the difference in decrease in PCE between the perovskite solar cells of different composition could be found. This might be attributed to the faster and slower phase segregation in $FA_{0.8}Cs_{0.2}Pb(I_{0.6}Br_{0.4})_3$ and $FA_{0.8}Cs_{0.2}Pb(I_{0.8}Br_{0.2})_3$ perovskites respectively.

As expected, by moving from a 20% to 40% bromide concentration in PSCs, it could also be observed that the V_{OC} increases, whereas the J_{SC} decreases. This behaviour is expected upon increasing the band gap. However, the decrease in J_{SC} and PCE over continuous illumination is not expected and can most likely be attributed to the phase segregation.

Nevertheless, there is still a lot of improvement needed in WBG perovskite solar cells. Further variation in additive concentration and application needs to be investigated to increase solar cell performance and to fully access the huge potential that WBG PSCs have in the photovoltaic industry.

5. List of Figures

6. List of Tables

7. References

[1] J. Goldemberg, World energy assessment. Energy and the challenge of sustainability, *UN*, **2001**, 235.

[2] J. F. Geisz, R. M. France, K. L. Schulte, M. A. Steiner, A. G. Norman, H. L. Guthrey, M. R. Young, T. Song, T. Moriarty, Six-junction III–V solar cells with 47.1% conversion efficiency under 143 Suns concentration, *Nature Energy*, **2020**, *5 (4)*, 326–335.

[3] L. Gao, I. Spanopoulos, W. Ke, S. Huang, I. Hadar, L. Chen, X. Li, G. Yang,M. G. Kanatzidis, *ACS Energy Lett.*, **2019**, *4*, 1763–1769.

[4] H. Min, D. Y. Lee, J. Kim, G. Kim, K. S. Lee, J. Kim, M. J. Paik, Y. K. Kim, K. S. Kim, M. G. Kim, T. J. Shin, S. I. Seok, *Nature*, **2021**, *598*, 444-463.

[5] NREL Transforming Energy, Best Research-Cell Efficiency Chart, URL: https://www.nrel.gov/pv/cell-efficiency.html, Accessed on: 07.11.2022

[6] G. Rose, Annalen der Physik **1839**, *124*, 558–561.

[7] Z. Cheng, J. Lin, *CrystEngComm*, **2010**, *12*, 2646–2662.

[8] Zijun Yi, et al., *Nanoscale Adv.***, 2019**,*1*, 1276-1289

[9] B. R. Nag, Physics of Quantum Well Devices, *Kluwer Academic Publishers*, Dordrecht, **2002**.

[10] B. Chen, P. N. Rudd, S. Yang, Y. Yuanc, J. Huang, *Chem. Soc. Rev.*, **2019**, *48*, 3842-3867.

[11] D. B. Khadka, Y. Shirai, M. Yanagida, T. Noda, K. Miyano, *ACS Appl. Mater. Interfaces*, **2018**, *10*, 22074–22082.

[12] M. Stolterfoht, C. M. Wolff, Y. Amir, A. Paulke, L. Perdigón-Toro, P. Caprioglio, D. Neher, *Energy Environ. Sci.*, **2017**, *10*, 1530–1539.

[13] K. A. Bush, K. Frohna, R. Prasanna, R. E. Beal, T. Leijtens, S. A. Swifter, M. D. McGehee, *ACS Energy Letters*, **2018**, *3 (2)*, 428-435.

[14] K. O. Brinkmann, T. Becker, F. Zimmermann, et al., Perovskite–organic tandem solar cells with indium oxide interconnect, *Nature*, **2022**, *604*, 280–286.

[15] W. Shockley, H. J. Queisser, *J. Appl. Phys.*, **1961**, *32*, 510–519.

[16] E. T. Hoke, D. J. Slotcavage, E. R. Dohner, A. R. Bowring, H. I. Karunadasa, M. D. McGehee, *Chem. Sci.*, **2015**, *6*, 613.

[17] Z. Li, T. H. Kim, S. Y. Han, Y. J. Yun, S. Jeong, B. Jo, S. A. Ok, W. Yim, S. H. Lee, K. Kim, S. Moon, J. Y. Park, T. K. Ahn, H. Shin, J. Lee, H. J. Park, *Adv. Energy Mater.*, **2020**, *10*, 1–16.

[18] G. E. Eperon, M. T. Hörantner, H. J. Snaith, Nat. Rev. Chem. **2017**, *1*, 1–18.

[19] S. Pöllner, A Processable and Efficient Perovskite Solar Cell with a Wide Band Gap, *Linz Institute of Organic Solar Cells*, **2022**.

[20] G. Yu, et al., *Solar Energy*, **2021**, *228*, 226-234

[21] M. Abdi-Jalebi, Z. Andaji-Garmaroudi, S. Cacovich, C. Stavrakas, B. Philippe, J. M. Richter, M. Alsari, E. P. Booker, E. M. Hutter, A. J. Pearson, S. Lilliu, T. J. Savenije, H. Rensmo, G. Divitini, C. Ducati, R. H. Friend, S. D. Stranks, *Nature*, **2018**, *555*, 497–501.

[22] T. I. Alanazi, O. S. Game, J. A. Smith, R. C. Kilbride, C. Greenland, R. Jayaprakash, K. Georgiou, N. J. Terrill, D. G. Lidzey, *RSC Adv.*, **2020**, *10*, 40341.

[23] Z. Liu, D. Liu, H. Chen, L. Ji, H. Zheng, Y. Gu, F. Wang, Z. Chen, S. Li, *Nanoscale Research Letters*, **2019**, *14*, 304.

[24] M. Lu, J. Guo, P. Lu, L. Zhang, Y. Zhang, Q. Dai, Y. Hu, V. L. Colvin, W. W. Yu, *J. Phys. Chem.*, **2019**, *123*, 22787−22792.

[25] J. Liang, C. Chen, X. Hu, Z. Chen, X. Zheng, J. Li, H. Wang, F. Ye, M. Xiao, Z. Lu, Y. Xu, S. Zhang, R. Yu, C. Tao, G. Fang, *ACS Appl. Mater. Interfaces*, **2020**, *12*, 48458−48466.

[26] Q. Jiang, Y. Zhao, X. Zhang, X. Yang, Y. Chen, Z. Chu, Q. Ye, X. Li, Z. Yin, J. You, *Nat. Photonics*, **2019**, *13*, 460–466.

[27] B. Hailegnaw, S. Paek, K. T. Cho, Y. Lee, F. Ongül, M. K. Nazeeruddin, M. C. Scharber, *Sol. RRL*, **2019**, 1900126.

[28] I. Poli, S. Eslava, P. Cameron, *J. Mater. Chem. A*, **2017**, *5*, 22325.

[29] C. L. Watts, L. Aspitarte, Y.-H. Lin, W. Li, R. Elzein, R. Addou, M. J. Hong, G. S. Herman, H. J. Snaith, J. G. Labram, *Communications Physics*, **2020**, *3*.

[30] K. Gugujonovic, Photoluminescence Enhancement in Perovskite Thin Films, *Linz Institute of Organic Solar Cells*, **2020**.

[31] R. J. Stoddard, Correlation between Photoluminescence and Carrier Transport and a Simple In Situ Passivation Method for High-Bandgap Hybrid Perovskites, *J. Phys. Chem. Lett.*, **2017**, *8*, 3289−3298.

[32] A. R. Zanatta, Revisiting the optical bandgap of semiconductors and the proposal of a unified methodology to its determination, *Sci. Rep.*, **2019**, *9*, 11225.